DEPT. OF MATH., UNIVERSITY OF OSLO
RESEARCH REPORT IN MECHANICS, No. 1
ISSN 0801-9940 February 2013
(Revised May 2014)

POST-BUCKLING AND ULTIMATE STRENGTH PREDICTION OF COMPOSITE PLATES USING A SEMI-ANALYTICAL METHOD

by

Qiao Jie Yang

Mechanics Division, Department of Mathematics,
University of Oslo

Abstract: Simply supported plates of laminated composite material subjected to uniaxial in-plane compression have been investigated. The ultimate strength analysis has been performed using a semi-analytical method based on large deflection theory and first order shear deformation theory. Two degradation models have been developed with material degradation either applied to the entire failed ply or to the affected regions of a failed ply. Both instantaneous and linear degradation of materials are presented. Further, two different types of in-plane displacement fields have been examined for their influence on the strength predictions.

Key words: Composite plates; Ultimate strength; Post-buckling; Hashin and Rotem failure criterion; Instantaneous material degradation; Linear material degradation.

CONTENTS

1 INTRODUCTION

1.1 Background

Plates made of fibre-reinforced composite materials are widely used in many structures, for example in certain types of ships and most wind turbine blades. In design of such large composite structures, buckling analysis is generally confined to estimation of elastic critical loads. For many plates, the carrying capacity can be significantly higher than the elastic critical load, while neglect of geometric imperfections in eigenvalue buckling analyses may result in overestimation of the strength. Thus, in order to include the post-buckling deformation and utilise the full potential of the material, ultimate strength analysis of such plates should be considered. Such analyses should also take account of geometric imperfections. For this, nonlinear finite element methods can be used, but are at present mostly restricted to research because these analyses tend to be complex and time consuming to prepare, run and post-process. Besides, commercial software sometimes has limitations, particularly with regard to material behaviour. In contrast, for plates made of steel material, design strength curves that take account of slenderness and geometric imperfections have been established based on extensive studies. For steel structures, practical, analytical and semi-analytical approaches for buckling and strength analysis are available; many of these are user-friendly and computationally efficient. However, these approaches are often tailor-made for specific cases for certain loads and boundary conditions, and are thus not so general as the FE method. Previously, to estimate the ultimate strength of stiffened and unstiffened thin steel plates under in-plane compression, Steen [1], Brubak *et al.* [2], and Brubak and Hellesland [3,4,5,6] have developed several simplified semi-analytical methods. The work reported here is part of a study that aims to extend these efficient methods to fibre-reinforced composite plates having a range of layups and thicknesses.

1.2 The Present Study

The present paper concerns the prediction of the ultimate strength of composite plates in compression using a semi-analytical method. As a first step to establish a more accurate, simplified and reliable method, several models based on small deflection theory, combined with first order shear deformations, have been presented in [7,8]. As expected, the investigation showed that neglect of non-linear post-buckling behaviour makes the ultimate strength estimations very conservative for thinner plates. For thicker plates, the results showed reasonable, but somewhat conservative predictions. As an extension of the previous work, the present method is able to take account of:

- failure and degradation models for composites,
- initial geometric imperfections,
- out-of-plane shear deformations which are most relevant for thick composite and sandwich plates, and
- post-buckling deformations, thus the reserve strength of plates which is especially important for thin plates.

As in [7,8], two different degradation approaches in combination with the Hashin and Rotem failure criterion [9] from 1973 have been used:

- Complete ply degradation model (CPDM): The material degradation is applied to entire plies.
- Ply region degradation model (PRDM): The stiffness degradation is limited to the affected regions of a failed ply.

For both approaches, an energy solution is performed using assumed deformations in the form of a truncated double Fourier series. For the PRDM, two types of assumed in-plane displacement fields have been investigated and both instantaneous and linear material degradation have been implemented. To validate the method, the results are compared with the FE analysis performed by Misirlis using ABAQUS, and reported by Hayman *et al.* [10].

2 BOUNDARY CONDITIONS AND DISPLACEMENTS

2.1 Kinematics

In order to describe the post-buckling behaviour, the classical large deflection theory (assumptions of moderate rotations, but small in-plane strains) combined with the first order shear deformation theory has been used. The nonlinear strains taking account of an initial out-of-plane imperfection w_{init} are given by [11,12]:

$$\varepsilon_{xx} = \varepsilon_{xx}^0 + z\kappa_{xx} = \left(\frac{\partial u_0}{\partial x} + \frac{1}{2}\left(\frac{\partial w}{\partial x} \right)^2 + \frac{\partial w}{\partial x}\frac{\partial w_{init}}{\partial x} \right) + z\left(\frac{\partial \phi_x}{\partial x} \right) \tag{1a}$$

$$\varepsilon_{yy} = \varepsilon_{yy}^0 + z\kappa_{yy} = \left(\frac{\partial v_0}{\partial y} + \frac{1}{2}\left(\frac{\partial w}{\partial y} \right)^2 + \frac{\partial w}{\partial y}\frac{\partial w_{init}}{\partial y} \right) + z\left(\frac{\partial \phi_y}{\partial y} \right) \tag{1b}$$

$$\gamma_{xy} = \gamma_{xy}^0 + z\kappa_{xy} = \left(\frac{\partial u_0}{\partial y} + \frac{\partial v_0}{\partial x} + \frac{\partial w}{\partial x}\frac{\partial w}{\partial y} + \frac{\partial w}{\partial x}\frac{\partial w_{init}}{\partial y} + \frac{\partial w}{\partial y}\frac{\partial w_{init}}{\partial x} \right) + z\left(\frac{\partial \phi_x}{\partial y} + \frac{\partial \phi_y}{\partial x} \right) \tag{1c}$$

$$\gamma_{xz} = \frac{\partial w}{\partial x} + \phi_x \tag{1d}$$

$$\gamma_{yz} = \frac{\partial w}{\partial y} + \phi_y \tag{1e}$$

Here x and y are the in-plane coordinates and z is the distance from the middle plane of the plate. The terms with the super index "0" denote the mid-plane membrane strains, while κ are the curvatures. The symbols u_0 and v_0 represent the mid-plane displacements in the x- and y-direction, respectively, while w is the out-of-plane displacement that is additional to the initial out-of-plane imperfection. The rotations of a transverse normal about axes parallel to the y and x axes are denoted by ϕ_x and ϕ_y, respectively.

2.2 Boundary Conditions and Displacement Field 1 (DF1)

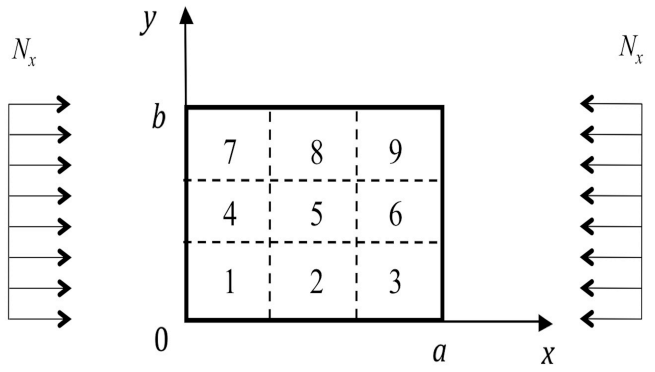

Fig. 1. Plate geometry and load condition. The broken lines and the numbers are explained in Section 6.2.

A rectangular plate is considered, with dimensions $a \times b$ (Fig. 1) with an initial out-of-plane deformation w_{init}. The plate is simply supported on all edges and subjected to a mean compression N_x in the x-direction. In the analyses, this is achieved by restraining the edge $x = 0$ in the x-direction and applying a uniform, negative displacement u_c in the x-direction on the edge $x = a$, all four edges being held straight. The total out-of-plane deformation is $w_{tot}=w_{init}+w$. Each deformation component is assumed in the form of a truncated double Fourier series [6,13] combined with a linear in-plane displacement field [6,14]:

$$u_0(x,y) = \sum_{n=1}^{N}\sum_{m=1}^{M} u_{mn} \sin\left(\frac{m\pi x}{a}\right)\sin\left(\frac{n\pi y}{b}\right) + u_c \frac{x}{a} \tag{2a}$$

$$v_0(x,y) = \sum_{n=1}^{N}\sum_{m=1}^{M} v_{mn} \sin\left(\frac{m\pi x}{a}\right)\sin\left(\frac{n\pi y}{b}\right) + v_c \frac{y}{b} \tag{2b}$$

$$\phi_x(x,y) = \sum_{n=1}^{N}\sum_{m=1}^{M} x_{mn} \cos\left(\frac{m\pi x}{a}\right)\sin\left(\frac{n\pi y}{b}\right) \tag{2c}$$

$$\phi_y(x,y) = \sum_{n=1}^{N}\sum_{m=1}^{M} y_{mn} \sin\left(\frac{m\pi x}{a}\right)\cos\left(\frac{n\pi y}{b}\right) \tag{2d}$$

$$\begin{aligned} w_{tot}(x,y) &= w(x,y) + w_{init}(x,y) \\ &= \sum_{n=1}^{N}\sum_{m=1}^{M} w_{mn} \sin\left(\frac{m\pi x}{a}\right)\sin\left(\frac{n\pi y}{b}\right) + \sum_{n=1}^{N}\sum_{m=1}^{M} w_{imn} \sin\left(\frac{m\pi x}{a}\right)\sin\left(\frac{n\pi y}{b}\right) \end{aligned} \tag{2e}$$

The coefficients u_c, v_c, u_{mn}, v_{mn}, x_{mn}, y_{mn} and w_{mn} are the unknowns, w_{imn} are given imperfection amplitudes, and m, n, M and N are positive integers.

2.3 Boundary Conditions and Displacement Field 2 (DF2)

For the second set of boundary conditions and assumed displacements, the out-of-plane displacement and the rotations are the same as those presented in Section 2.2, i.e. Eqs. (2c)-(2e), but the in-plane displacement fields are replaced by those used by Reddy [10] for simply supported plates:

$$u_0(x,y) = \sum_{n=1}^{N}\sum_{m=1}^{M} u_{mn} \sin\left(\frac{m\pi x}{a}\right)\cos\left(\frac{n\pi y}{b}\right) + u_c \frac{x}{a} \tag{3a}$$

$$v_0(x,y) = \sum_{n=1}^{N}\sum_{m=1}^{M} v_{mn} \cos\left(\frac{m\pi x}{a}\right)\sin\left(\frac{n\pi y}{b}\right) + v_c \frac{y}{b} \tag{3b}$$

Note that the linear in-plane displacement fields are unchanged, and all four edges are still constrained to remain straight, but the displacement component u_0 is now allowed to vary more freely along the edges $y = 0,b$ and v_0 is allowed to vary more freely along the edges $x = 0,a$. Note that for odd values of m or n, the cosine terms in DF2 give an antisymmetric variation along or across the plate. Reddy primarily applied DF2 for antisymmetric *angle-ply* laminates having ply orientations of θ and $-\theta$ where $0° \le \theta \le 90°$, and having at least one layer with an orientation other than 0° or 90°.

3 POTENTIAL ENERGY

The total potential energy consists of three contributions associated, respectively, with in-plane strain energy, shear strain energy and external forces:

$$\Pi = U_p + U_s + U_f \tag{4}$$

The strain energy associated with in-plane stresses can be written as

$$\begin{aligned} U_p &= \frac{1}{2}\int_V \varepsilon_p^T \sigma_p \, dV = \frac{1}{2}\int_A \int_{-h/2}^{h/2} \varepsilon_p^T \bar{Q} \varepsilon_p \, dz \, dA \\ &= \frac{1}{2}\int_A \left[\left(\varepsilon^0\right)^T A \varepsilon^0 + 2\left(\varepsilon^0\right)^T B\kappa + \kappa^T D\kappa \right] dA \\ &= U_m + U_{mb} + U_b \end{aligned} \tag{5}$$

where U_m and U_b are the membrane and bending strain energies, respectively, and U_{mb} is the strain energy due to the coupling terms between the membrane and bending contributions.

$$\begin{aligned} U_m = \frac{1}{2}\int_A \left(\varepsilon^0\right)^T A \varepsilon^0 dA = \frac{1}{2}\int_0^b \int_0^a \Big[& A_{11}\left(\varepsilon_{xx}^0\right)^2 + 2A_{12}\varepsilon_{xx}^0\varepsilon_{yy}^0 + A_{22}\left(\varepsilon_{yy}^0\right)^2 \\ & + 2A_{16}\varepsilon_{xx}^0\gamma_{xy}^0 + 2A_{26}\varepsilon_{yy}^0\gamma_{xy}^0 + A_{66}\left(\gamma_{xy}^0\right)^2 \Big] dx dy \end{aligned} \tag{6a}$$

$$U_{mb} = \frac{1}{2}\int_A 2\left(\varepsilon^0\right)^T B\kappa dA = \int_0^b\int_0^a \Big[B_{11}\varepsilon_{xx}^0\kappa_{xx} + B_{12}\left(\varepsilon_{xx}^0\kappa_{yy} + \varepsilon_{yy}^0\kappa_{xx}\right) + B_{22}\varepsilon_{yy}^0\kappa_{yy}$$

$$+B_{16}\left(\varepsilon_{xx}^0\kappa_{xy} + \gamma_{xy}^0\kappa_{xx}\right) + B_{26}\left(\varepsilon_{yy}^0\kappa_{xy} + \gamma_{xy}^0\kappa_{yy}\right) + B_{66}\gamma_{xy}^0\kappa_{xy}\Big] dxdy \tag{6b}$$

$$U_b = \frac{1}{2}\int_A \kappa^T D\kappa dA = \frac{1}{2}\int_0^b\int_0^a \Big[D_{11}\left(\kappa_{xx}\right)^2 + 2D_{12}\kappa_{xx}\kappa_{yy} + D_{22}\left(\kappa_{yy}\right)^2$$

$$+2D_{16}\kappa_{xx}\kappa_{xy} + 2D_{26}\kappa_{yy}\kappa_{xy} + D_{66}\left(\kappa_{xy}\right)^2\Big] dxdy \tag{6c}$$

The extensional stiffness matrix is given by A, while B and D are the bending-stretching coupling matrix and the bending stiffness matrix, respectively.

The transverse shear strain is given in Eq. (7):

$$U_s = \frac{1}{2}\int_V \varepsilon_s^T\sigma_s dV = \frac{1}{2}\int_A \int_{-h/2}^{h/2} \varepsilon_s^T \overline{Q}_s\varepsilon_s\, dz\, dA = \frac{1}{2}\int_A \varepsilon_s^T A_s\varepsilon_s dA$$

$$= \frac{1}{2}k\int_0^b\int_0^a \left[A_{44}\left(\phi_y + \frac{\partial w}{\partial y}\right)^2 + A_{55}\left(\phi_x + \frac{\partial w}{\partial x}\right)^2\right] dxdy \tag{7}$$

Here, A_s is the stiffness matrix for transverse shear and k (= 5/6) is the shear correction coefficient.

For nonlinear analysis, it is most convenient to introduce a dimensionless load parameter Λ, and define N_x as a constant reference load value, which is chosen based on the laminate thicknesses. The potential energy of an external, in-plane load ΛN_x in the x-direction is given by

$$U_f = \Lambda N_x b u_c \tag{8}$$

where b is the width of the plate.

4 SOLUTION PROCEDURE

4.1 Incremental Response Propagation

The post-buckling response is traced by an incremental procedure [1]. Here, an arc length parameter is used as a propagation parameter.

Using large deflection theory, the equilibrium equations obtained from the Rayleigh-Ritz method are nonlinear. Instead of solving the nonlinear equations directly, these are solved incrementally by computing the rate form of the equilibrium equations with respect to an arc length parameter η. Further, the change in the arc length parameter is

associated with a change in the external load and the displacements and rotations. For an external applied load, changing proportionally with Λ, this relationship is illustrated graphically in Fig. 2.

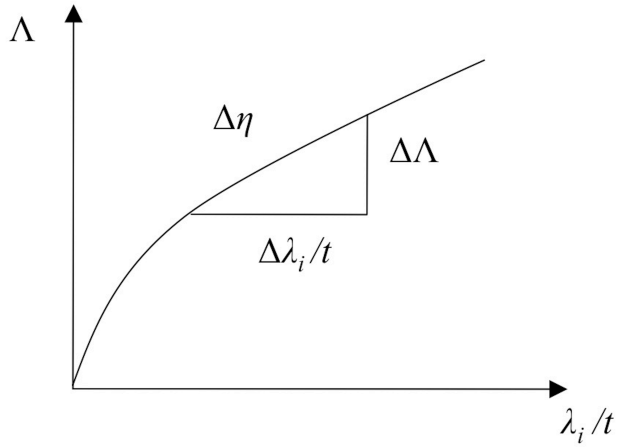

Fig. 2. Relationship between an arc length parameter increment $\Delta\eta$, a load increment $\Delta\Lambda$ and an incremental displacement amplitude $\Delta\lambda_i$.

As the increment size approaches zero, the relationship can be given by

$$
\begin{aligned}
&(\Delta\Lambda)^2 + \left(\frac{\Delta\lambda_i}{t}\right)^2 = (\Delta\eta)^2 \\
\Rightarrow &\left(\frac{\Delta\Lambda}{\Delta\eta}\right)^2 + \frac{1}{t^2}\left(\frac{\Delta\lambda_i}{\Delta\eta}\right)^2 = 1 \\
\Rightarrow &\left(\frac{\partial\Lambda}{\partial\eta}\right)^2 + \frac{1}{t^2}\left(\frac{\partial\lambda_i}{\partial\eta}\right)^2 = 1 \\
\Rightarrow &\dot{\Lambda}^2 + \sum_{Displ.}\frac{\dot{\lambda}_i^2}{t^2} + \sum_{Rot.}\dot{\lambda}_i^2 = 1
\end{aligned}
\tag{9}
$$

where λ_i represents the displacement and rotation amplitudes and t is the plate thickness. A dot above a symbol can be interpreted as differentiation with respect to the arc length parameter η.

In the incremental procedure, the load parameter Λ and displacement and rotation amplitudes λ_i are functions of the arc length parameter η. For an increment $\Delta\eta$ along the equilibrium curve from point s to (s +1), a Taylor series expansion gives

$$\lambda_i^{s+1} = \lambda_i^s + \dot{\lambda}_i^s\Delta\eta + \frac{1}{2}\ddot{\lambda}_i^s\Delta\eta^2 + \ldots \tag{10a}$$

$$\Lambda^{s+1} = \Lambda^s + \dot{\Lambda}^s\Delta\eta + \frac{1}{2}\ddot{\Lambda}^s\Delta\eta^2 + \ldots \tag{10b}$$

The second and higher order terms are neglected in the present work, i.e. the expansion is of first order. In other works, such as in Byklum [15], it is shown how to include the second order terms. However, by choosing a sufficiently small increment, the results achieved by this first order expansion are found to be satisfactory. Besides, retaining the second or higher order terms to improve the accuracy is computationally costly.

4.2 Incremental Equilibrium Equations

The Rayleigh-Ritz method on an incremental form or rate form as mentioned in Section 4.1 has been used to solve the problem. The total potential energy is given by Eq. (4). Equilibrium requires that $\delta\dot{\Pi} = 0$, and thus

$$\frac{\partial\dot{\Pi}}{\partial\lambda_i} = \frac{\partial}{\partial\eta}\left(\frac{\partial\Pi}{\partial\lambda_i}\right) = \frac{\partial}{\partial\lambda_i}\left(\frac{\partial\Pi}{\partial\eta}\right) = \frac{\partial}{\partial\lambda_i}\left(\frac{\partial\Pi}{\partial\lambda_j}\right)\frac{\partial\lambda_j}{\partial\eta} + \frac{\partial}{\partial\lambda_i}\left(\frac{\partial\Pi}{\partial\Lambda}\right)\frac{\partial\Lambda}{\partial\eta}$$
$$= \frac{\partial^2\Pi}{\partial\lambda_i\partial\lambda_j}\dot{\lambda}_j + \frac{\partial^2\Pi}{\partial\lambda_i\partial\Lambda}\dot{\Lambda} = C_{ij}\dot{\lambda}_j + F_i\dot{\Lambda} = 0 \tag{11}$$

Here, C_{ij} is a generalised, incremental stiffness matrix and $F_i\dot{\Lambda}$ is a generalised, incremental load vector, where i indicates the row number and j the column number in a matrix. The total number of unknowns is $N_{tot} + 1$ (λ_i and Λ), where N_{tot} is number of equations in Eq. (11). The additional equation required is Eq. (9). In matrix form, Eq. (11) becomes:

$$\begin{bmatrix}
\frac{\partial^2\Pi}{\partial u_c\partial u_c} & \frac{\partial^2\Pi}{\partial u_c\partial v_c} & \frac{\partial^2\Pi}{\partial u_c\partial u_{ij}} & \frac{\partial^2\Pi}{\partial u_c\partial v_{ij}} & \frac{\partial^2\Pi}{\partial u_c\partial x_{ij}} & \frac{\partial^2\Pi}{\partial u_c\partial y_{ij}} & \frac{\partial^2\Pi}{\partial u_c\partial w_{ij}} \\
\frac{\partial^2\Pi}{\partial v_c\partial u_c} & \frac{\partial^2\Pi}{\partial v_c\partial v_c} & \frac{\partial^2\Pi}{\partial v_c\partial u_{ij}} & \frac{\partial^2\Pi}{\partial v_c\partial v_{ij}} & \frac{\partial^2\Pi}{\partial v_c\partial x_{ij}} & \frac{\partial^2\Pi}{\partial v_c\partial y_{ij}} & \frac{\partial^2\Pi}{\partial v_c\partial w_{ij}} \\
\frac{\partial^2\Pi}{\partial u_{fg}\partial u_c} & \frac{\partial^2\Pi}{\partial u_{fg}\partial v_c} & \frac{\partial^2\Pi}{\partial u_{fg}\partial u_{ij}} & \frac{\partial^2\Pi}{\partial u_{fg}\partial v_{ij}} & \frac{\partial^2\Pi}{\partial u_{fg}\partial x_{ij}} & \frac{\partial^2\Pi}{\partial u_{fg}\partial v_{ij}} & \frac{\partial^2\Pi}{\partial u_{fg}\partial w_{ij}} \\
\frac{\partial^2\Pi}{\partial v_{fg}\partial u_c} & \frac{\partial^2\Pi}{\partial v_{fg}\partial v_c} & \frac{\partial^2\Pi}{\partial v_{fg}\partial u_{ij}} & \frac{\partial^2\Pi}{\partial v_{fg}\partial v_{ij}} & \frac{\partial^2\Pi}{\partial v_{fg}\partial x_{ij}} & \frac{\partial^2\Pi}{\partial v_{fg}\partial y_{ij}} & \frac{\partial^2\Pi}{\partial v_{fg}\partial w_{ij}} \\
\frac{\partial^2\Pi}{\partial x_{fg}\partial u_c} & \frac{\partial^2\Pi}{\partial x_{fg}\partial v_c} & \frac{\partial^2\Pi}{\partial x_{fg}\partial u_{ij}} & \frac{\partial^2\Pi}{\partial x_{fg}\partial v_{ij}} & \frac{\partial^2\Pi}{\partial x_{fg}\partial x_{ij}} & \frac{\partial^2\Pi}{\partial x_{fg}\partial y_{ij}} & \frac{\partial^2\Pi}{\partial x_{fg}\partial w_{ij}} \\
\frac{\partial^2\Pi}{\partial y_{fg}\partial u_c} & \frac{\partial^2\Pi}{\partial y_{fg}\partial v_c} & \frac{\partial^2\Pi}{\partial y_{fg}\partial u_{ij}} & \frac{\partial^2\Pi}{\partial y_{fg}\partial v_{ij}} & \frac{\partial^2\Pi}{\partial y_{fg}\partial x_{ij}} & \frac{\partial^2\Pi}{\partial y_{fg}\partial y_{ij}} & \frac{\partial^2\Pi}{\partial y_{fg}\partial w_{ij}} \\
\frac{\partial^2\Pi}{\partial w_{fg}\partial u_c} & \frac{\partial^2\Pi}{\partial w_{fg}\partial v_c} & \frac{\partial^2\Pi}{\partial w_{fg}\partial u_{ij}} & \frac{\partial^2\Pi}{\partial w_{fg}\partial v_{ij}} & \frac{\partial^2\Pi}{\partial w_{fg}\partial x_{ij}} & \frac{\partial^2\Pi}{\partial w_{fg}\partial y_{ij}} & \frac{\partial^2\Pi}{\partial w_{fg}\partial w_{ij}}
\end{bmatrix}$$

$$\cdot\begin{bmatrix} \dot{u}_c \\ \dot{v}_c \\ \dot{u}_{ij} \\ \dot{v}_{ij} \\ \dot{x}_{ij} \\ \dot{y}_{ij} \\ \dot{w}_{ij} \end{bmatrix} + \begin{bmatrix} \dfrac{\partial^2 \Pi}{\partial u_c \partial \Lambda} \\ \dfrac{\partial^2 \Pi}{\partial v_c \partial \Lambda} \\ \dfrac{\partial^2 \Pi}{\partial u_{fg} \partial \Lambda} \\ \dfrac{\partial^2 \Pi}{\partial v_{fg} \partial \Lambda} \\ \dfrac{\partial^2 \Pi}{\partial x_{fg} \partial \Lambda} \\ \dfrac{\partial^2 \Pi}{\partial y_{fg} \partial \Lambda} \\ \dfrac{\partial^2 \Pi}{\partial w_{fg} \partial \Lambda} \end{bmatrix} \cdot \dot{\Lambda} = 0 \tag{12}$$

The row number is indicated by *f* and *g* for corresponding displacement and rotation amplitudes with two subscripts. Further, in a similar way, *i* and *j* are used to indicate the column number.

4.3 Procedure for Solving the Equations

First, $\dot{\lambda}_j$ and $\dot{\Lambda}$ can be found by solving the Eqs. (9) and (11). The solution of Eq. (11) is given by

$$\dot{\lambda}_j = -\dot{\Lambda} C_{ij}^{-1} F_i \tag{13}$$

Substituting equation (13) into equation (9):

$$\dot{\Lambda}^2 \left(t^2 + \sum_{Displ.} \left(C_{ij}^{-1} F_i \right)^2 + t^2 \sum_{Rot.} \left(C_{ij}^{-1} F_i \right)^2 \right) = t^2 \tag{14}$$

Then, from Eq. (14), the load rate parameter $\dot{\Lambda}$ can be determined as

$$\dot{\Lambda} = \pm \frac{t}{\sqrt{t^2 + \sum_{Displ.} \left(C_{ij}^{-1} F_i \right)^2 + t^2 \sum_{Rot.} \left(C_{ij}^{-1} F_i \right)^2}} \tag{15}$$

Based on the assumption that the equilibrium curve is smooth, it is necessary to find the solution to Eq. (15) that gives a continuous increase of the arc length. This is achieved by the requirement that the absolute value of the angle between the tangents of the

consecutive increments ($s-1$) and s in the load-displacement space is smaller than 90°. For the correct sign of the load rate $\dot{\Lambda}^s$ at stage s, the following equivalent criterion must be satisfied [1]:

$$\dot{\Lambda}^s \left(\frac{\sum_{Displ.} \left(-C_{ij}^{-1} F_i\right)^s \dot{\lambda}_j^{s-1}}{t^2} + \sum_{Rot.} \left(-C_{ij}^{-1} F_i\right)^s \dot{\lambda}_j^{s-1} + \dot{\Lambda}^{s-1} \right) > 0 \tag{16}$$

When $\dot{\Lambda}^s$ at stage s is found, the displacement and rotation rate amplitudes $\dot{\lambda}_j^s$ at the stage s are given by Eq. (13). The displacement and rotation amplitudes, and load parameter at the next stage are then obtained by the first order Taylor series expansion:

$$\lambda_j^{s+1} = \lambda_j^s + \dot{\lambda}_j^s \Delta\eta \tag{17a}$$

$$\Lambda^{s+1} = \Lambda^s + \dot{\Lambda}^s \Delta\eta \tag{17b}$$

As mentioned in section 4.1, $\Delta\eta$ has to be small to give a satisfactory result. The solution propagation is continued until a given failure criterion is reached.

4.4 Application of Riks-Wempner Method

The method described in Section 4.3 has the major advantage of its simplicity in application. However, the major drawback of the method is that the unbalanced forces occurring in each load increment are ignored, i.e. no iterations are performed to bring the calculated equilibrium path back to the true one. These existing errors tend to accumulate and eventually become significant, sometimes leading to convergence problems. To reduce these errors, it is necessary to arrange an iterative procedure within each load increment to correct for the disagreement that exists between the external applied forces and the internal forces of the system. A way to perform this iteration is by using the Riks-Wempner method [16,17].

In order to apply the Riks-Wempner method, Eq. (11) has been modified to include the unbalanced forces U_i [18,19]:

$$C_{ij}\dot{\lambda}_j + F_i\dot{\Lambda} + U_i = 0 \tag{18}$$

Eq. (18) can be decomposed into two equations:

$$-\dot{\Lambda} C_{ij}^{-1} F_i = \dot{\Lambda}\bar{\dot{\lambda}}_j \tag{19a}$$

$$-C_{ij}^{-1} U_i = \bar{\bar{\dot{\lambda}}}_j \tag{19b}$$

Here, Eq. (19a) gives the displacement and rotation increments associated with the generalised, incremental load vector provided in Eq. (13), while Eq. (19b) gives the displacement and rotation increments associated with the unbalanced forces. Note that

for the sake of convenience, the displacement increments presented in this section are assumed to be dimensionless.

For the first iteration at a randomly selected load step s, $\left\{\dot{\Lambda}^s\right\}^1$ and $\left\{\dot{\lambda}_j^s\right\}^1$ are found by following the solution procedure described in Section 4.3 (the unbalanced forces are zero in the beginning), and in turn $\left\{\Lambda^{s+1}\right\}^1$ and $\left\{\lambda_j^{s+1}\right\}^1$ are obtained by using Eqs. (17). The unbalanced forces based on the predicted displacement and rotation amplitudes and load parameter are thus

$$U_i^r = \left(\frac{\partial \Pi}{\partial \lambda_i}\right)^r = H_{ij}\left\{\lambda_j^{s+1}\right\}^r - \left\{\Lambda^{s+1}\right\}^r L_j, \quad r \geq 1 \tag{20}$$

Here, r denotes iteration number, H_{ij} is a stiffness matrix and L_j is a load vector.

For subsequent iterations at the same load step s, the load incremental factor $\left\{\dot{\Lambda}^s\right\}^r$ is determined by enforcing the orthogonality condition [18]:

$$\left\{\dot{\Lambda}^s\right\}^1\left\{\dot{\Lambda}^s\right\}^r + \sum_{j=1}^{N_{tot}}\left(\left\{\dot{\lambda}_j^s\right\}^1\right)^T\left\{\dot{\lambda}_j^s\right\}^r = 0, \quad r > 1 \tag{21}$$

The corrected version of displacement and rotation increments $\left\{\dot{\lambda}_j^s\right\}^r$ can be calculated by superposition based on Eqs. (19):

$$\left\{\dot{\lambda}_j^s\right\}^r = \left\{\dot{\Lambda}^s\overline{\dot{\lambda}_j^s}\right\}^r + \left\{\overline{\overline{\dot{\lambda}_j^s}}\right\}^r, \quad r > 1 \tag{22}$$

Substituting for $\left\{\dot{\lambda}_j^s\right\}^1$ and $\left\{\dot{\lambda}_j^s\right\}^r$ using Eq. (19a) and Eq. (22), Eq. (21) becomes

$$\left\{\dot{\Lambda}^s\right\}^1\left\{\dot{\Lambda}^s\right\}^r + \sum_{j=1}^{N_{tot}}\left(\left\{\dot{\Lambda}^s\overline{\dot{\lambda}_j^s}\right\}^1\right)^T\left(\left\{\dot{\Lambda}^s\overline{\dot{\lambda}_j^s}\right\}^r + \left\{\overline{\overline{\dot{\lambda}_j^s}}\right\}^r\right) = 0, \quad r > 1 \tag{23}$$

Solving Eq. (23) for $\left\{\dot{\Lambda}^s\right\}^r$ gives

$$\left\{\dot{\Lambda}^s\right\}^r = -\frac{\sum_{j=1}^{N_{tot}}\left(\left\{\overline{\dot{\lambda}_j^s}\right\}^1\right)^T\left\{\overline{\overline{\dot{\lambda}_j^s}}\right\}^r}{1+\sum_{j=1}^{N_{tot}}\left(\left\{\overline{\dot{\lambda}_j^s}\right\}^1\right)^T\left\{\overline{\dot{\lambda}_j^s}\right\}^r}, \quad r > 1 \tag{24}$$

Finally, the load and displacement and rotation increments at stage s are given by

$$\dot{\Lambda}^s = \sum_{r=1}^{\infty} \left\{ \dot{\Lambda}^s \right\}^r \tag{25a}$$

$$\dot{\lambda}_j^s = \sum_{r=1}^{\infty} \left\{ \dot{\lambda}_j^s \right\}^r \tag{25b}$$

A schematic illustration of the method is presented in Fig. 3.

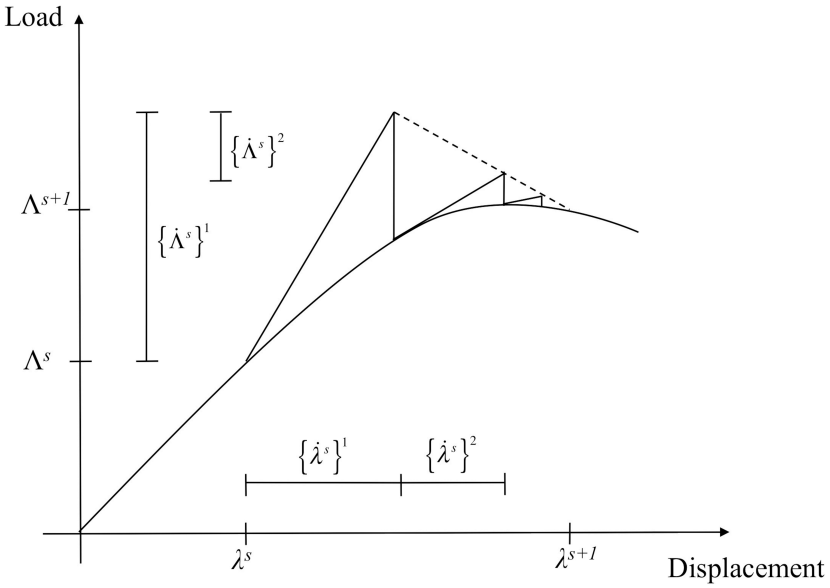

Fig. 3. Iterations performed by the Riks-Wempner method.

A convergence criterion must be introduced to determine the number of iterations needed to reduce the errors within each load step. This criterion is based on the magnitude of the unbalanced forces U and the internal forces I [19,20]:

$$\|U\| < \beta \|I\| \tag{26}$$

In the analyses performed in Section 7, the chosen value of β is 0.01.

The Riks-Wempner method has only been implemented after damage initiation in the analyses with linear degradation of the material properties. In the analyses implemented with the instantaneous material degradation model, an unloading and reloading technique is used (see Fig. 5 in Section 5.3.2), which compensates for the absence of an iterative procedure within each load increment.

5 PROGRESSIVE FAILURE MODELS

5.1 Hashin and Rotem Failure Criterion

The 1973 Hashin and Rotem failure criterion for in-plane stresses can be written [9]:

$$f_1^T = \left(\frac{\sigma_{11}}{X_t}\right)^2 = 1 \;;\; f_2^T = \left(\frac{\sigma_{22}}{Y_t}\right)^2 + \left(\frac{\tau_{12}}{S_{12}}\right)^2 = 1 \tag{27a}$$

$$f_1^C = \left(\frac{\sigma_{11}}{X_c}\right)^2 = 1 \;;\; f_2^C = \left(\frac{\sigma_{22}}{Y_c}\right)^2 + \left(\frac{\tau_{12}}{S_{12}}\right)^2 = 1 \tag{27b}$$

Failure occurs when any of the four failure functions from Eqs. (27) reaches unity. Each is associated with a dominant failure mode.

5.2 Degradation of Properties

When failure occurs in a laminated composite plate, the effective material properties change. This results in a new stiffness of the plate. To describe this behaviour, a damaged material stiffness matrix for in-plane deformations is defined [10]:

$$[R] = \begin{bmatrix} (1-d_1)R_{11} & (1-d_1)(1-d_2)R_{12} & 0 \\ sym. & (1-d_2)R_{22} & 0 \\ sym. & sym. & (1-d_6)R_{66} \end{bmatrix} \tag{28}$$

Here d_1 is the damage factor in the longitudinal direction of the material, d_2 is the damage factor in the transverse direction, and d_6 is the damage factor in the in-plane shear component. The remaining parameters in Eq. (28) are defined as $R_{11} = \frac{E_1}{\Delta}$, $R_{22} = \frac{E_2}{\Delta}$, $R_{12} = \frac{\nu_{12}E_2}{\Delta}$, $R_{66} = G_{12}$ and $\Delta = 1 - \nu_{12}\nu_{21}(1-d_1)(1-d_2)$.

For the Hashin criterion, because the shear failure component is associated with the fibre and matrix modes of failure, the damage variable d_6 is defined as:

$$d_6 = 1 - (1-d_1)(1-d_2) \tag{29}$$

To allow direct comparison with the results of Misirlis [10], the transverse (out-of-plane) shear stiffness matrix is not degraded during the analysis. (The ABAQUS shell elements used by Misirlis do not allow such degradation of the transverse shear properties.) Thus

$$[K] = \begin{bmatrix} K_{44} & 0 \\ 0 & K_{55} \end{bmatrix} \tag{30}$$

where $K_{44} = G_{23}$ and $K_{55} = G_{13}$.

5.3 Material Degradation

5.3.1 Introduction

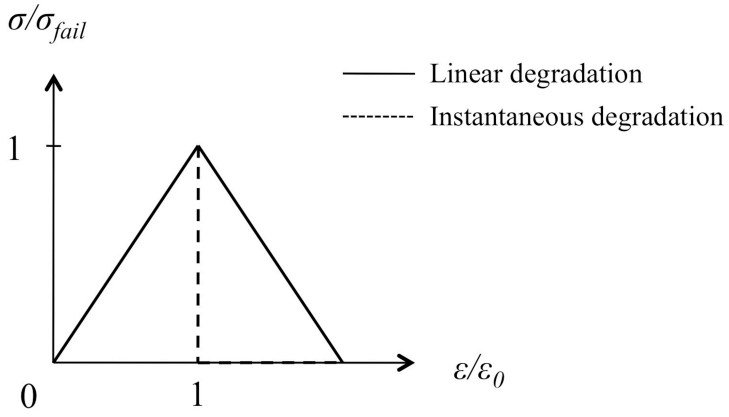

Fig. 4. Material degradations.

Both instantaneous degradation and linear degradation of material properties are implemented in the progressive failure model reported here, see Fig. 4 [21]. The FEA results presented in Hayman *et al.* [10] assumed a linear degradation of the properties by using the built-in progressive failure model in ABAQUS.

5.3.2 Instantaneous Material Degradation

For the instantaneous material degradation, when any ply or ply region fulfils a stress criterion, its corresponding properties are instantaneously reduced to a predefined value equal to 1% of the respective initial values [22]. Thus the associated damage factor d_i = 0.99. The analyses implemented with the instantaneous material degradation are performed with the unloading and reloading technique, which is illustrated in Fig. 5. After damage is detected in a ply or a ply region, the plate is unloaded and material degradation is applied. The plate is then reloaded with the reduced material stiffness until further damage is detected. This process is repeated until appearance of the ultimate load.

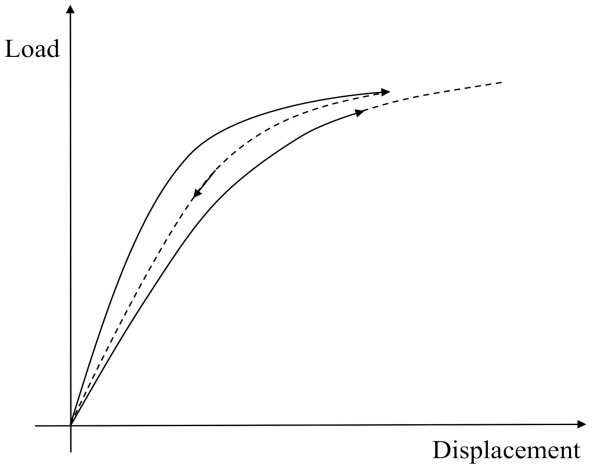

Fig. 5. The unloading and reloading procedure associated with the instantaneous material degradation.

5.3.3 Linear Material Degradation

For linear degradation of the material properties, the degradation procedure is based on the constitutive model proposed by Matzenmiller *et al.* [21], i.e. the damage evolution is similar to the model implemented in ABAQUS. More information is given in Appendix A [23]. In each of the failure modes provided in Eqs. (27), a damage variable d_i will evolve based on the stress-displacement relation shown in Fig. A.1 and Eq. (A.5) in Appendix A. This stress-displacement behaviour is expressed as equivalent stress σ_{eq} and equivalent displacement δ_{eq}, where δ_{eq}^{0} is the initial equivalent displacement at which the initiation criterion for that mode was met and δ_{eq}^{f} is the displacement at which the material is completely damaged in this failure mode. Further, δ_{eq}^{f} is given as;

$$\delta_{eq}^{f} = \alpha \delta_{eq}^{0} \tag{31}$$

For both matrix and fibre failure modes, $\alpha = 2$ [21] has been used in most of the cases investigated in Section 7. In section 7.8.2, a lower α value has been applied for the fibre failure modes. Note that the ABAQUS analyses were performed with $\alpha = 2$ for all failure modes.

6 DEGRADATION MODELS

6.1 Complete Ply Degradation Model (CPDM)

In the complete ply degradation model (CPDM), if any part of a ply has exceeded a given stress criterion, degradation of the corresponding properties is applied to that entire ply. The plate is analysed under increasing loads using the equations and procedures described in the previous sections. In the analyses presented here using CPDM, only the displacement field described in Section 2.2 has been considered. The degradation procedure is shown schematically in Fig. 6. The process is repeated until the maximum value of load is reached; this is considered to be the ultimate load.

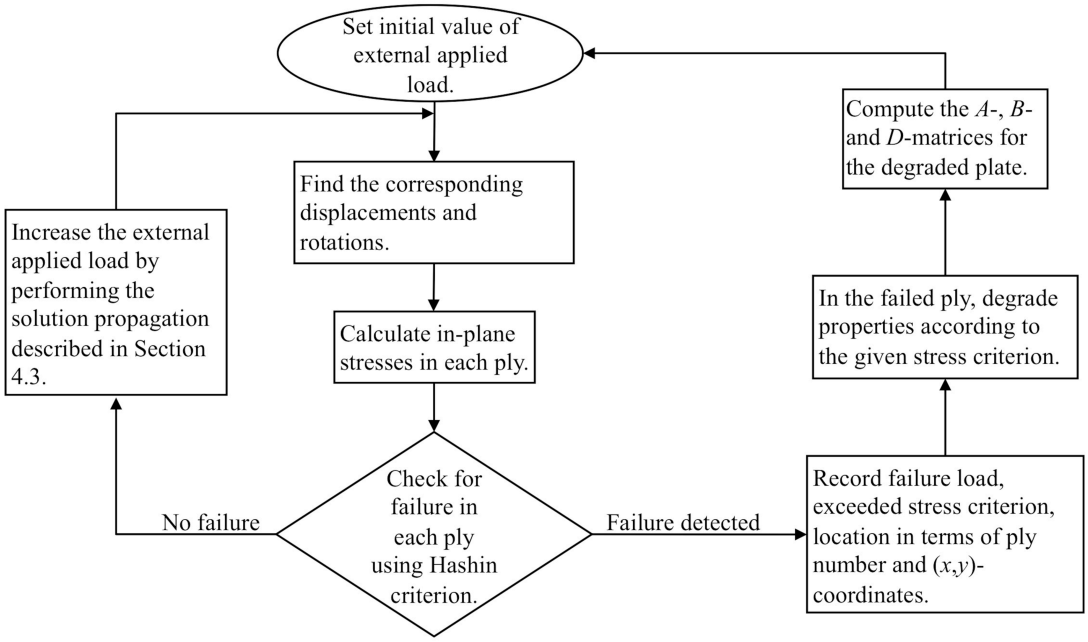

Fig. 6. Schematic diagram: procedure for both CPDM and PRDM with the instantaneous material degradation. The procedure is repeated until maximum load is reached.

6.2 Ply Region Degradation Model (PRDM)

To use the ply region degradation model (PRDM) the plate is divided into 9 regions as shown by the broken lines in Fig. 1. Thus regions 1, 3, 7 and 9 are corner regions, 5 is a centre region and 2, 4, 6 and 8 are mid-edge regions (of which 4 and 6 are loaded edges). The progressive failure model with degraded material properties is now implemented by reducing the appropriate stiffness terms only in the specific region of the ply where failure has occurred. This model has the advantage that it allows a closer approximation to the true degradation distribution, while also giving some useful insight into the dominant failure mechanisms and sequences. In the analyses with PRDM, the two alternative displacement fields presented in Sections 2.2 and 2.3 have been considered. Otherwise, the procedure implemented with the instantaneous material degradation is similar to the CPDM (Fig. 6). The procedure implemented with the linear material degradation and the Riks-Wempner method is presented in Fig. 7.

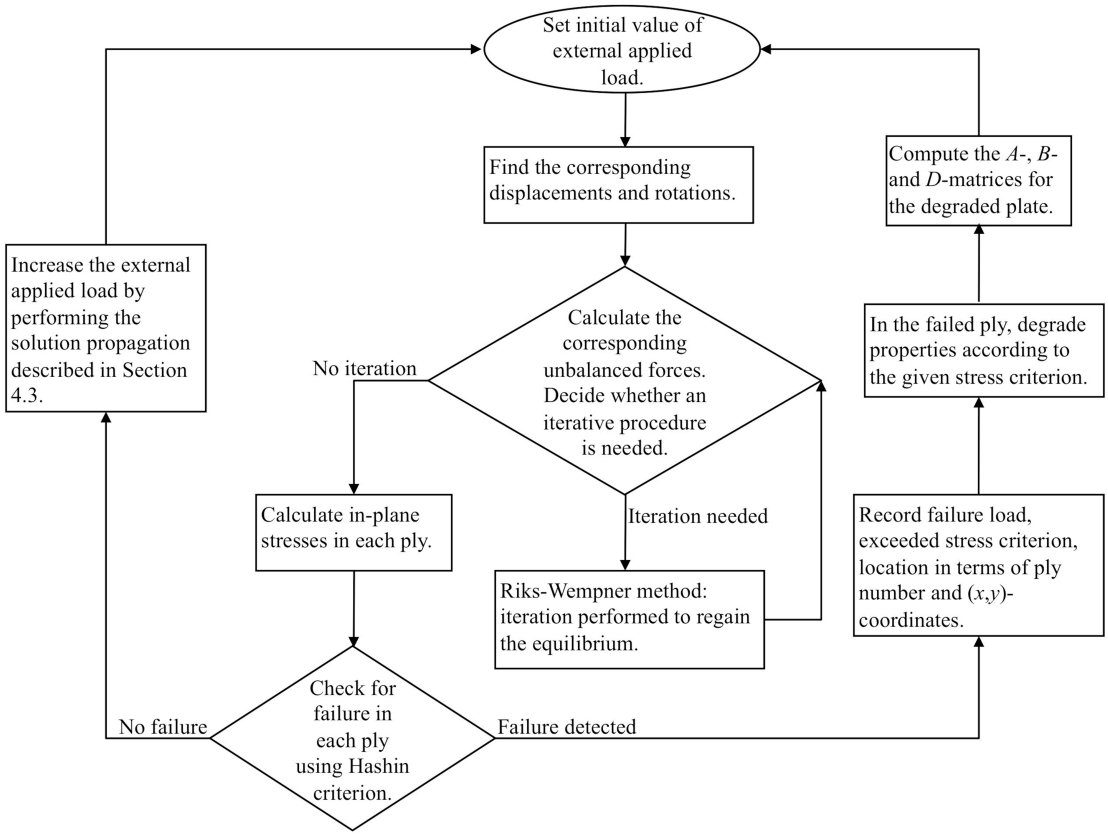

Fig. 7. Schematic diagram: procedure for PRDM with the linear material degradation. The procedure is repeated until maximum load is reached.

7 PARAMETRIC STUDY

7.1 Description

To test the simplified approach by comparing results with those obtained by Misirlis using advanced FE analysis [10], parametric studies have been performed for a series of square plates, with $a = b = 500$ mm, having various breadth/thickness (b/t) ratios. Four different maximum initial imperfection amplitudes have been examined, respectively 0.1%, 1%, 2% and 3% of the width b (= 500 mm). The assumed shape of the initial geometric imperfection is a single half sine wave in each direction, so that $w_{imn} = 0$ for all values of m and n other than 1. Two different types of composite layup are considered [10]:

- Case A, a triaxial layup: $\left[-45/+45/0_4/+45/-45/0_4/-45/+45/0_3\right]_S$
  This layup configuration is typical for the main spar of a wind turbine blade.
- Case B, a quasi-isotropic, quadriaxial layup: $\left[0/+45/90/-45\right]_{X,S}$
  This layup configuration is more typical for ship hull panels that experience a mixture of lateral pressure and in-plane loading due to hull girder bending.

For the triaxial layups (case A), the required b/t values are achieved by scaling the thickness of each individual ply. For the quadriaxial layups (case B), the thickness is increased by adding groups of plies (increasing X) to give the desired b/t values. The

material properties and the plate thicknesses for cases A and B are given in Tables 1-3. Note that ply number 1 is located on the concave side of the plate. It should be mentioned that Misirlis [24] observed that in some cases the linear degradation model overestimated the ultimate strength, so validation against other sources is also needed. Furthermore, the layup configurations considered are two extreme cases; in order to have a better overall picture of the trends, other layups have been evaluated in Section 7.9. For the ply region degradation model (see Fig. 1), regions 1, 3, 7 and 9 are each 160 mm × 160 mm, regions 2 and 8 are each 180 mm × 160 mm, regions 4 and 6 are 160 mm × 180 mm and region 5 is 180 mm × 180 mm.

Table 1
Material properties (strengths and moduli).

Property	E_1	E_2	ν_{12}	G_{12}	G_{13}	G_{23}	X_t	X_c	Y_t	Y_c	S_{12}
Value	49627	15430	0.272	4800	4800	4800	968	915	24	118	65
Units	MPa	MPa	-	MPa	MPa	MPa	MPa	MPa	MPa	MPa	MPa

Table 2
Plate thicknesses and ply thicknesses for case A.

Layup case	b/t	t (mm)	t_0 (mm)	$t_{\pm 45}$ (mm)
A1	50	10.00	0.39	0.12
A2	30	16.70	0.65	0.20
A3	20	25.00	0.97	0.30
A4	15	33.30	1.30	0.40
A5	10	50.00	1.95	0.59

Table 3
Plate thicknesses and ply thicknesses for case B.

Layup case	b/t	t (mm)	X	t_0, $t_{\pm 45}$, t_{90} (mm)
B1	62.50	8.00	1	1.00
B2	31.25	16.00	2	1.00
B3	20.83	24.00	3	1.00
B4	15.63	32.00	4	1.00
B5	10.42	48.00	6	1.00

7.2 Step Size and Number of Terms

The physical step size along the equilibrium path is dependent on the chosen propagation parameter value $\Delta\eta$ and the chosen size of the load interval, which in turn depends on the selected value of N_x. In order to reduce the computation time, larger propagation parameter values may be considered. The influence of the step size $\Delta\eta$ on the accuracy of ultimate strength estimations is presented in Fig. 8. The total number of increments used in a calculation is given as the inverse of the propagation parameter, $1/\Delta\eta$. The ultimate strengths are plotted relative to an ultimate strength $\sigma_{\max,100}$ estimated with a small value of $\Delta\eta = 0.01$ ($1/\Delta\eta = 100$). In most of the cases investigated, $\Delta\eta = 0.10$ was found to give reasonably accurate results with acceptable computational time. More information regarding the chosen N_x and $\Delta\eta$ values is given in Appendix C and D. Note that the influence of the chosen step size $\Delta\eta$ will only affect the models without Riks-Wempner method. More explanation is given in Section 4.4.

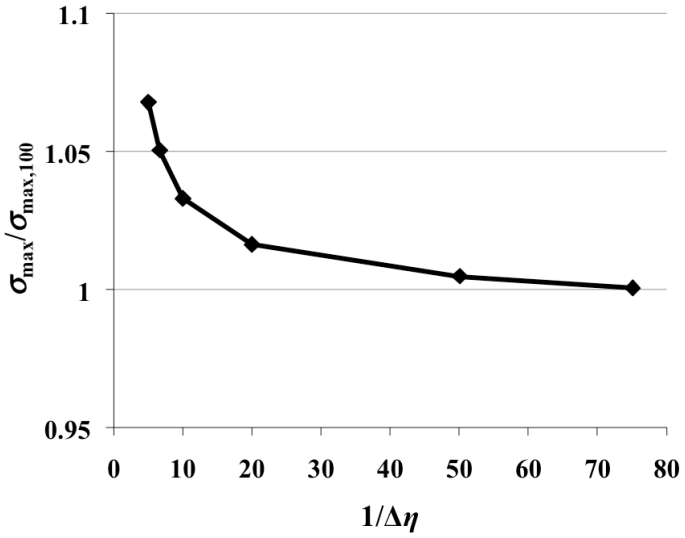

Fig. 8. The ultimate strength relation is plotted against $1/\Delta\eta$ for layup A3 (in Table 2) with 1% imperfection using CPDM.

A convergence test (Tables B.1-B.3 in Appendix B) has been performed to determine the total number of terms to be used in the assumed displacement fields given by Eqs. (2) and (3). In this test, the number of terms is increased until the change of result is less than 1%.

7.3 Load-Displacement Response Without Material Degradation

The load-displacement responses for plates with various thicknesses and imperfection amplitudes are provided in Figs. 9-14. Without material degradation, a reasonable load-displacement response is achieved with 127 terms included in the displacement fields presented in Eqs. (2). The results have been compared to FE analyses performed in ANSYS with chosen element type SHELL281 and element size 25×25 mm^2.

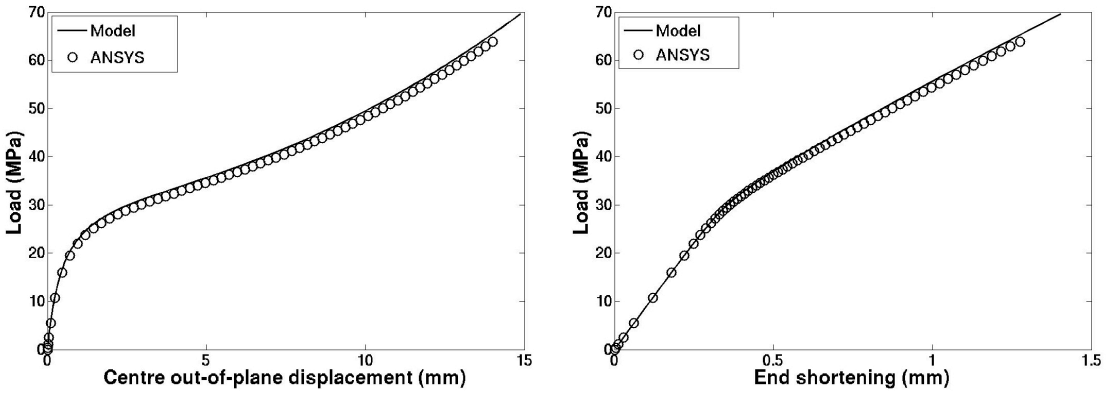

Fig. 9. Load vs. centre out-of-plane displacement (left) and load vs. end shortening (right) for case A, t = 10.02 mm and 0.1% imperfection. The line shows the results from the present method and the circles are the results form ANSYS.

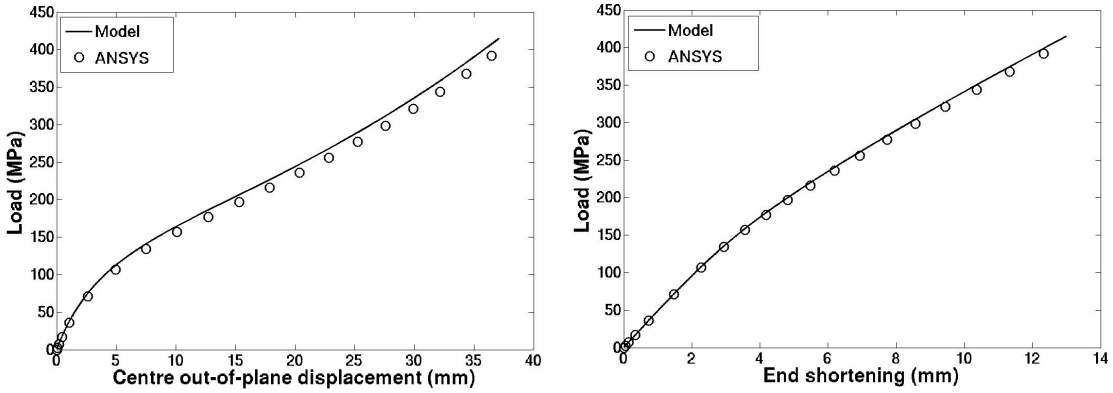

Fig. 10. Load vs. centre out-of-plane displacement (left) and load vs. end shortening (right) for case A, t = 10.02 mm and 1% imperfection. The line shows the results from the present method and the circles are the results from ANSYS.

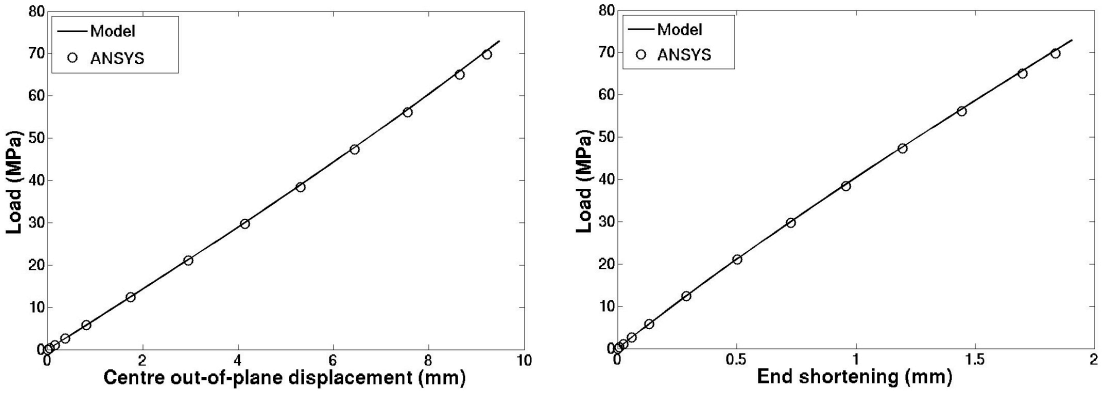

Fig. 11. Load vs. centre out-of-plane displacement (left) and load vs. end shortening (right) for case A, t = 10.02 mm and 3% imperfection. The line shows the results from the present method and the circles are the results from ANSYS.

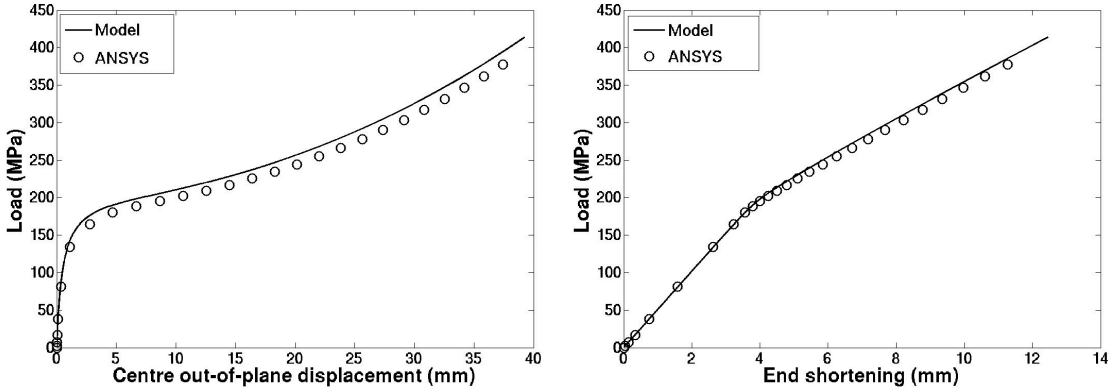

Fig. 12. Load vs. centre out-of-plane displacement (left) and load vs. end shortening (right) for case B, t = 24 mm and 0.1% imperfection. The line shows the results from the present method and the circles are the results from ANSYS.

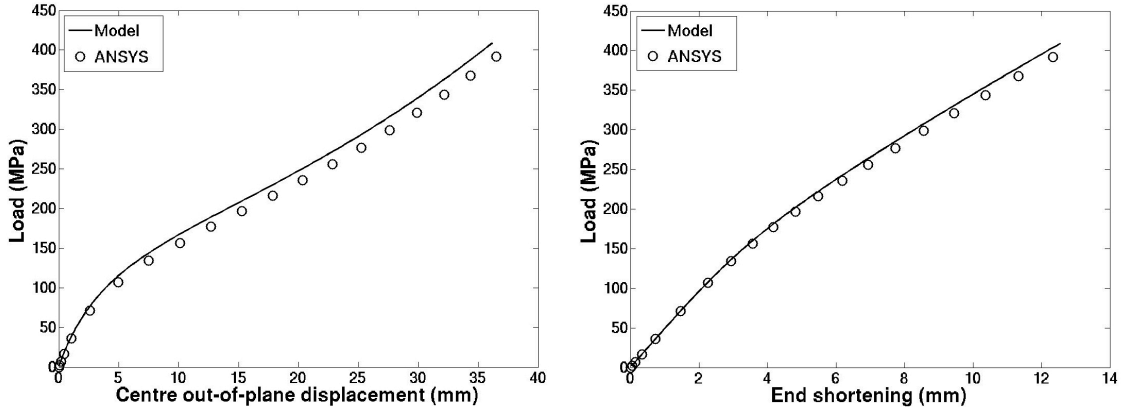

Fig. 13. Load vs. centre out-of-plane displacement (left) and load vs. end shortening (right) for case B, t = 24 mm and 1% imperfection. The line shows the results from the present method and the circles are the results from ANSYS.

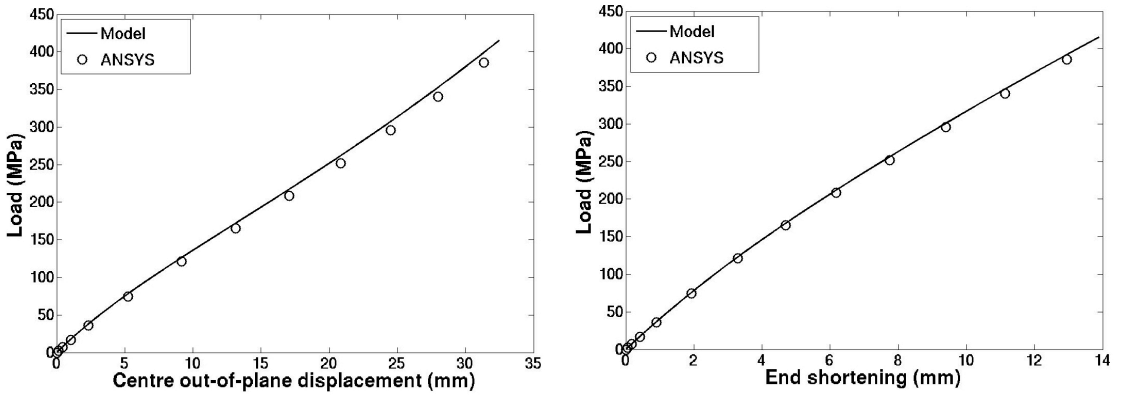

Fig. 14. Load vs. centre out-of-plane displacement (left) and load vs. end shortening (right) for case B, t = 24 mm and 3% imperfection. The line shows the results from the present method and the circles are the results from ANSYS.

From Figs. 9-14, the present method gives slightly greater plate stiffness than the ANSYS results, especially in the post-buckling area. This could be explained by the fact that the element type SHELL281 in ANSYS uses reduced integration in the calculations. Compared with ANSYS, the load vs. end shortening curves produce a better agreement than the load vs. centre out-of-plane displacement curves.

7.4 CPDM with Instantaneous Material Degradation

The detailed results using CPDM for a limited number of cases are given in Appendix C, Tables C.1-C.2 for layup cases A and B, respectively. The ratios of the ultimate strengths estimated using the present model to the reference values found by Misirlis are shown in Figs. 15-16 for various values of plate thickness t and imperfection amplitude.

For the triaxial layup, case A, the outermost 0° plies on the convex side of the plate undergo matrix failure first for all cases except for the thickest plate (A5 in Table 2) with 0.1% imperfection. For that layup, matrix failure occurs in the outermost -45° ply on the concave side of the plate. For the case A layups generally, the 0° plies usually

fail first in the centre of the plate, while the ±45° plies fail at the corners. The total number of plies is 34 for case A, and all 34 plies experience matrix failure before the ultimate strength is reached at the first incidence of fibre failure. This trend is seen for all cases, regardless of thickness or imperfection. From Table C.1, the ultimate strength predictions using CPDM are in the range of 14% - 33% smaller than Misirlis's FE analysis. The greatest deviations are observed for the thin plates (A1).

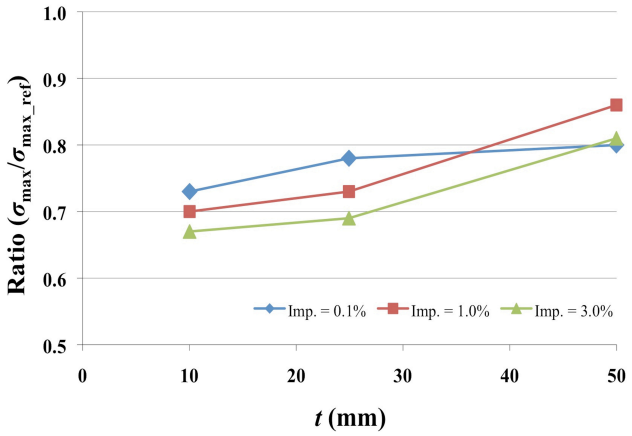

Fig. 15. Case A (triaxial layup) with complete ply degradation model: the ultimate strengths from the present analyses are compared to the reference values σ_{max_ref} obtained by Misirlis [10], for various plate thicknesses t and imperfection amplitudes.

For the quadriaxial layup, case B, first ply failure occurred as matrix failure in the outermost 0° plies on the convex side of the plate for all cases except for the thickest plate (B5 in Table 3) with 0.1% imperfection. For that layup, matrix failure occurred in the outermost 90° ply on the concave side of the plate. In general, the 0° and 90° plies tend to fail first in the centre of the plate, while the ±45° plies fail at the corners. According to Table C.2, for this more balanced layup configuration, the ultimate strength predictions using CPDM are 11% - 21% lower than Misirlis's ABAQUS results. This range of deviations is smaller than for case A layups, and with less variation. For all cases except the thickest plate (B5) with 0.1% and 1% imperfections, all plies experience matrix failure and the ultimate strength is reached at the first, or sometimes the second, occurrence of fibre failure. For layup B5 with 0.1% imperfection, all ±45° plies experienced matrix failure before the occurrence of the ultimate strength; this is reached at the first incidence of fibre failure, which occurs in a 0° ply without matrix failure. A similar trend is observed for layup B5 with 1% imperfection. However, this time all ±45° plies as well as some of the 0° plies experience matrix failure before the occurrence of the ultimate strength, which is again at the first fibre failure, occurring in a 0° ply without matrix failure.

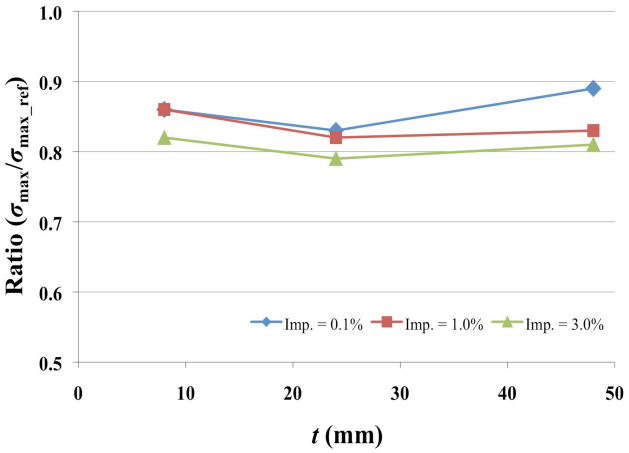

Fig. 16. Case B (quadriaxial layup) with complete ply degradation model: the ultimate strengths from the present analyses are compared to the reference values σ_{max_ref} obtained by Misirlis [10], for various plate thicknesses t and imperfection amplitudes.

7.5 PRDM-DF1 with Instantaneous Material Degradation

The corresponding results using PRDM-DF1 are provided in Figs. 17-18 and Tables C.3-C.4 in Appendix C for a limited number of cases. For both layup cases, considering first ply failure, there is no detectable difference between CPDM and PRDM-DF1, as should be expected. The matrix failures occurred in the same locations at the same calculated stresses.

For case A layups, the ultimate strength predictions using PRDM-DF1 are in the range 14% - 29% smaller than Misirlis's FE analysis. Again, the deviations are smallest for the thickest plate (A5). Further, no clear trend is observed except that at least 90% of the ply regions experience matrix failure before the ultimate strength is attained at the first fibre failure. For layup A5 with 1% imperfection, the ultimate strength is reached at the first incidence of fibre failure, occurring in a ply region without matrix failure.

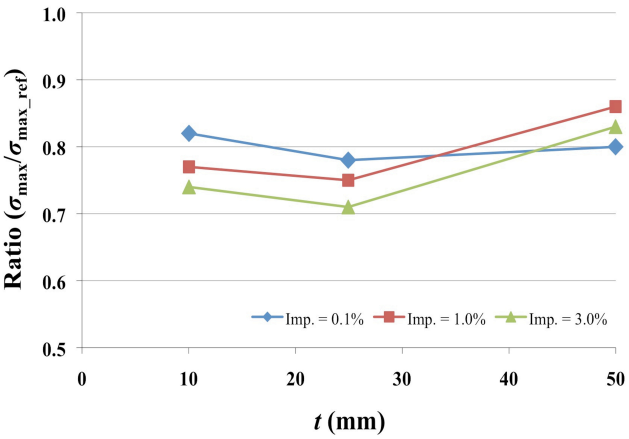

Fig. 17. Case A (triaxial layup) with ply region degradation model (DF1): the ultimate strengths from the present analyses are compared to the reference values σ_{max_ref} obtained by Misirlis, for various plate thicknesses t and imperfection amplitudes.

For case B layups, the ultimate strength predictions using PRDM-DF1 are 3% - 19% lower than the ABAQUS results provided by Misirlis, which for some of the cases is appreciably better than the predictions with CPDM. The best results are achieved for a thin plate (B1). For case B layups, 75% of the ply regions and 95% of the ply regions suffer matrix failure before the ultimate strength is attained at the first and second fibre failure, respectively, for layups B3 and B1. For layup B5, the trend is similar to that with CPDM; 75% - 90% of ply regions experience matrix failure before the first incidence of fibre failure, which occurs in a ply region without matrix failure, gives the ultimate strength.

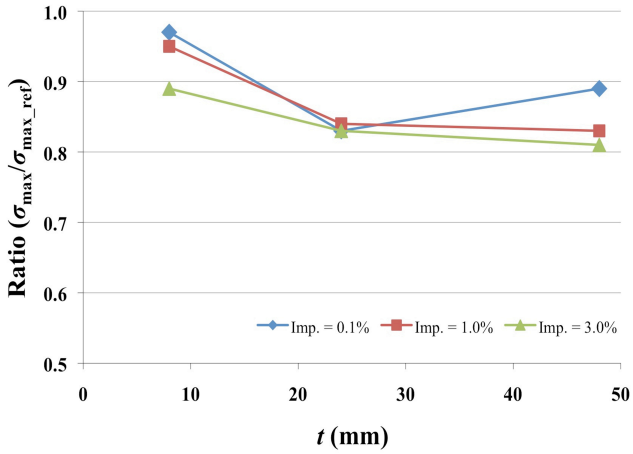

Fig. 18. Case B (quadriaxial layup) with ply region degradation model (DF1): the ultimate strengths from the present analyses are compared to the reference values σ_{max_ref} obtained by Misirlis, for various plate thicknesses t and imperfection amplitudes.

7.6 PRDM-DF2 with Instantaneous Material Degradation

The results using PRDM-DF2 are provided in Figs. 19-20 and Tables C.5-C.6 in Appendix C for a limited number of cases. For both layup cases, considering first ply failure, PRDM-DF2 provides higher predictions than PRDM-DF1, but the matrix failures occur in the same plies.

For case A layups, the ultimate strength predictions using PRDM-DF2 are still 3% - 20% smaller than those from Misirlis's FE analysis. The greatest improvements obtained by using displacement field 2 are found for layup A3, for which the sequence of failures is changed. Fibre failure now occurs in the ply regions without matrix failure. With DF1, this behaviour was limited to layup A5. For layup A1, the improvements are about 0% - 7% compared to PRDM-DF1, while the results are almost unchanged for thick plates. The ultimate strength is reached at the first occurrence of fibre failure for all analyses of case A layups using PRDM-DF2.

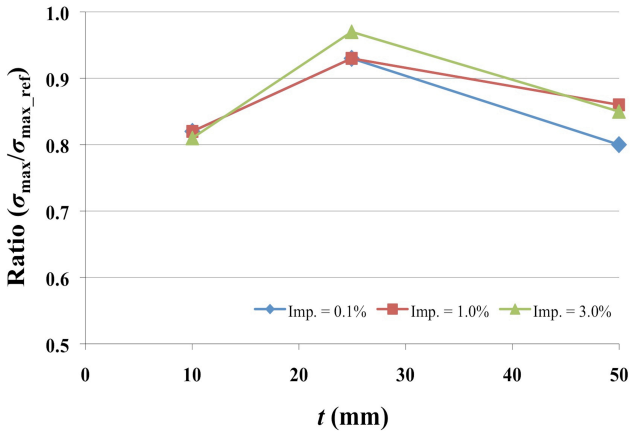

Fig. 19. Case A (triaxial layup) with ply region degradation model (DF2): the ultimate strengths from the present analyses are compared to the reference values σ_{max_ref} obtained by Misirlis, for various plate thicknesses *t* and imperfection amplitudes.

For case B layups, the ultimate strength predictions using PRDM-DF2 range from 2% higher to 25% lower than Misirlis's ABAQUS results. By using the displacement field 2, the strength estimations have *decreased* for moderately thick and thick plates compared to the results achieved by PRDM-DF1. The results for case B layups have thus become more consistent with those for case A layups. A special case has also been found for a moderately thick plate with 0.1% imperfection: the ultimate strength is reached at first ply failure. For thin plates, significant improvements are observed and the strength predictions are now almost identical to the ABAQUS results. As with PRDM-DF1, the ultimate strength predicted for thin plates occurred at the second incidence of fibre failure. For the remaining analyses, the first occurrence of fibre failure gives the ultimate load.

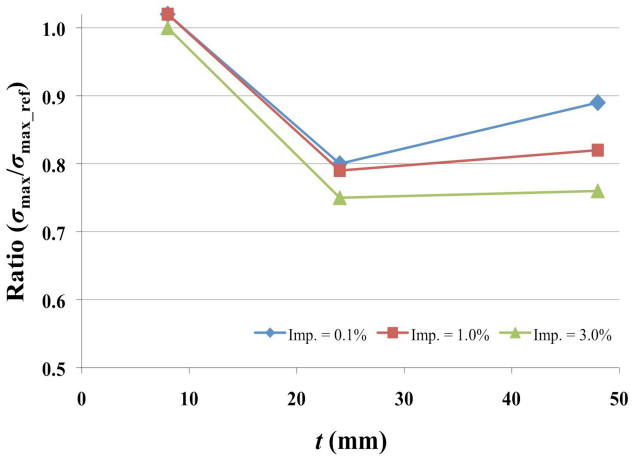

Fig. 20. Case B (quadriaxial layup) with ply region degradation model (DF2): the ultimate strengths from the present analyses are compared to the reference values σ_{max_ref} obtained by Misirlis, for various plate thicknesses *t* and imperfection amplitudes.

7.7 PRDM-DF1 with Linear Material Degradation

7.7.1 Ultimate Strength Predictions

The results using PRDM-DF1 with linear material degradation are provided in Figs. 21-24 and in full detail in Appendix D, Tables D.1-D.2 for layup cases A and B, respectively. In Figs. 22 and 24, the ultimate strength for a range of b/t values is presented along with the corresponding results presented by Misirlis. These figures include ultimate loads (squash loads) for extremely thick plates ($b/t < 10$), which has been found by using the present method with $b/t = 5$ and initial geometric imperfection equal to 0.002% of the plate width. The critical buckling loads for various b/t values estimated from a linear eigenvalue analysis are also provided in the same figures.

For case A layups, the ultimate strengths predicted are in the range 0% - 26% smaller than Misirlis's FE analysis. Implementation with the linear material degradation gives a desirable increase of ultimate strengths compared to the results produced by the instantaneous material degradation for most of the cases. The greatest deviations are found for layups A2 and A3. For layup A3 with 0.1% imperfection, the strength estimation has *decreased* compared to the similar case in Section 7.5. From Fig. 22, the strength predictions from the present model and ABAQUS indicate very little dependence on the imperfection amplitudes for b/t values greater than 25. It can also be seen that the elastic critical load is a rather conservative estimate of the ultimate strength for b/t values greater than about 20, with the current analysis indicating a transition at a slightly lower b/t value than that of Misirlis.

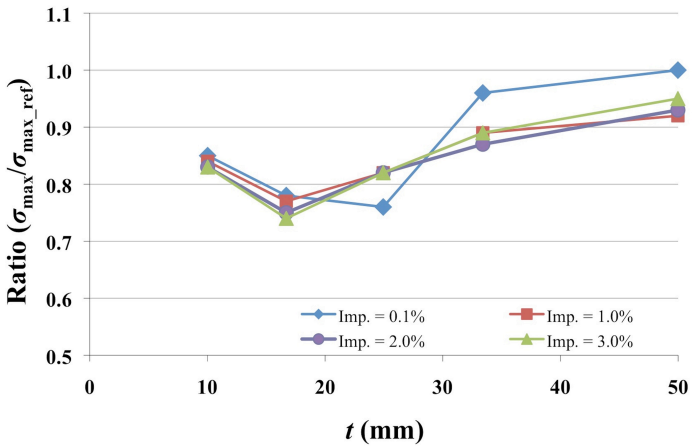

Fig. 21. Case A (triaxial layup) with ply region degradation model (DF1): the ultimate strengths from the present analyses are compared to the reference values σ_{max_ref} obtained by Misirlis, for various plate thicknesses t and imperfection amplitudes.

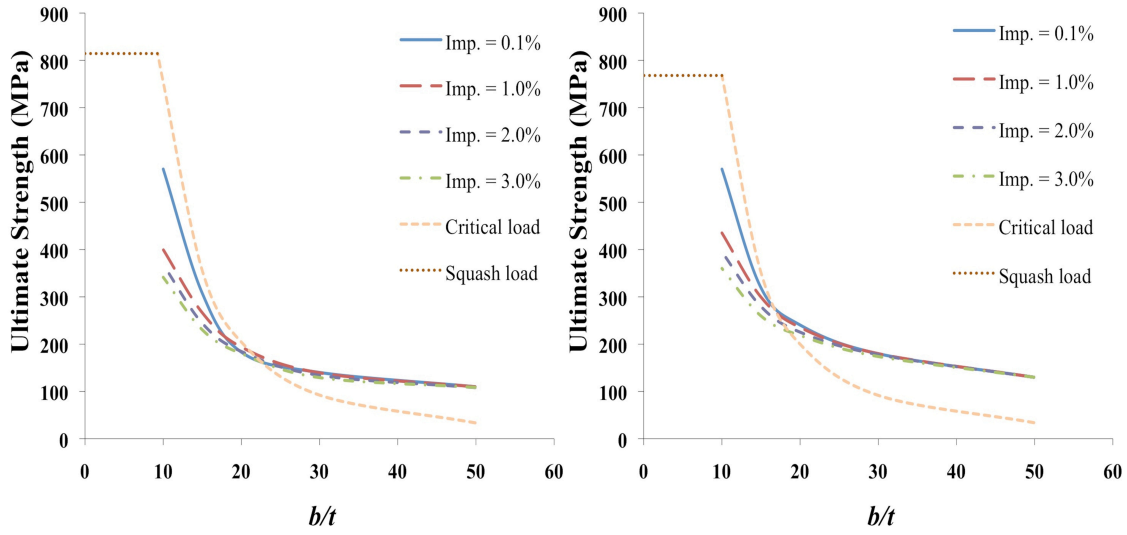

Fig. 22. Case A (triaxial layup) with ply region degradation model (DF1): the ultimate strengths from the present analyses (left) are compared to the corresponding results obtained by Misirlis (right) [10], for various *b*/*t* values and imperfection amplitudes.

For case B layups, the ultimate strength predictions range from 3% higher to 15% lower than the ABAQUS results provided by Misirlis. As expected, the linear degradation of material properties provides appreciably greater plate stiffness than the predictions with the instantaneous material degradation. The best results are achieved for thin plates. For this balanced layup configuration, the present model produced a more stable deviation than case A layups. From Fig. 24, case B layups appear to have little sensitivity to initial imperfections in the *b*/*t* region greater than 30 according to the present analysis or 25 according Misirlis's ABAQUS results. Considering the elastic critical load, the curve is located significantly lower than the corresponding strength predictions for *b*/*t* values greater than 22-23 for both the present model and the results presented by Misirlis.

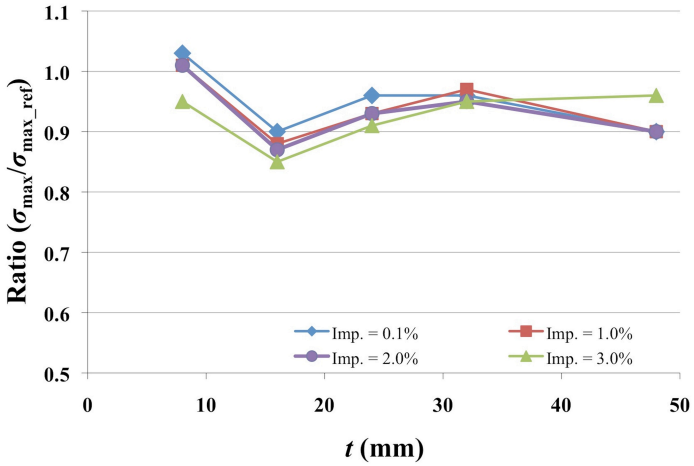

Fig. 23. Case B (quadriaxial layup) with ply region degradation model (DF1): the ultimate strengths from the present analyses are compared to the reference values σ_{max_ref} obtained by Misirlis, for various plate thicknesses *t* and imperfection amplitudes.

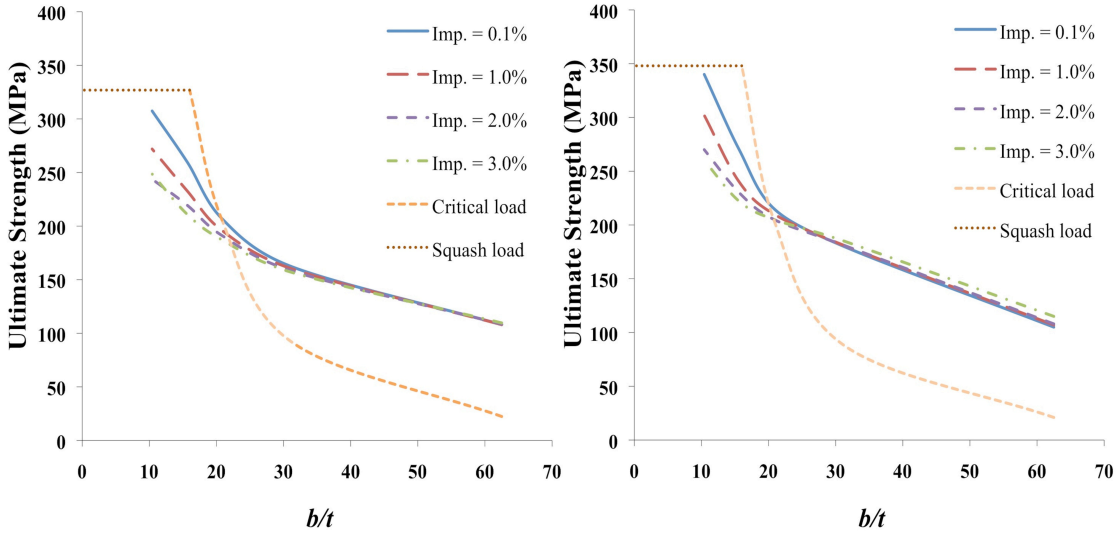

Fig. 24. Case B (quadriaxial layup) with ply region degradation model (DF1): the ultimate strengths from the present analyses (left) are compared to the corresponding results obtained by Misirlis (right) [10], for various b/t values and imperfection amplitudes.

7.7.2 Load-Displacement Response

For a limited number of cases, the load-displacement responses using the linear material degradation model and the instantaneous material degradation model are shown in Figs. 25-27. Instantaneous degradation of the material properties results in a more severe reduction in plate stiffness, so that more conservative ultimate strengths are achieved for this model.

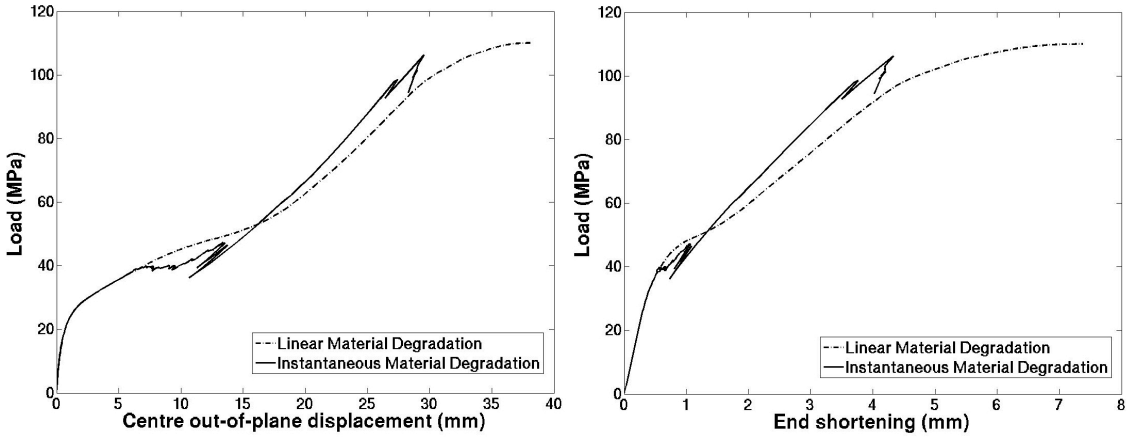

Fig. 25. Load vs. centre out-of-plane displacement (left) and load vs. end shortening (right) for case A (triaxial layup) with t = 10.02 mm and 0.1% imperfection amplitude.

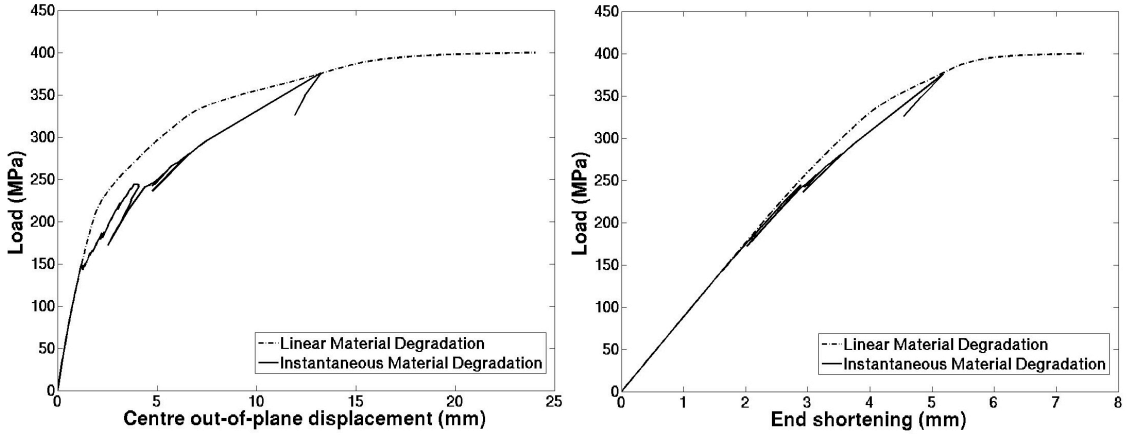

Fig. 26. Load vs. centre out-of-plane displacement (left) and load vs. end shortening (right) for case A (triaxial layup) with t = 49.98 mm and 1% imperfection amplitude.

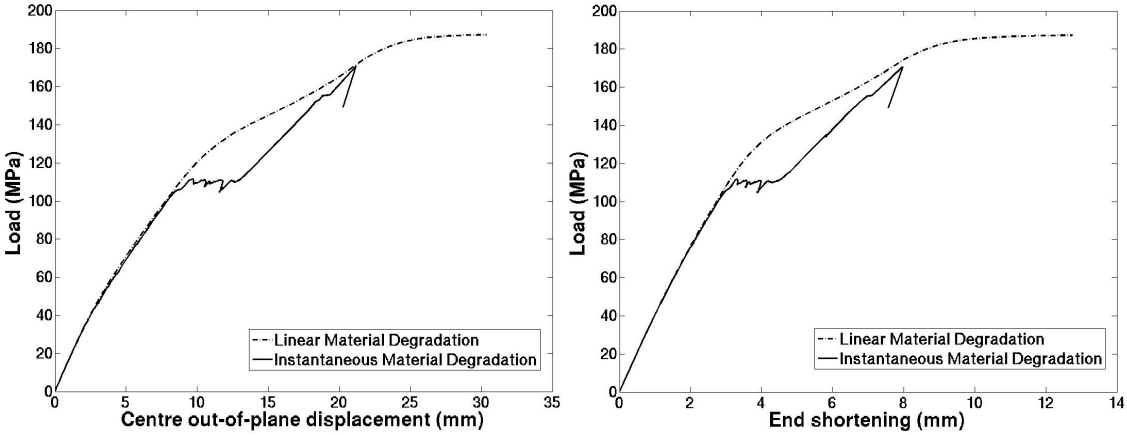

Fig. 27. Load vs. centre out-of-plane displacement (left) and load vs. end shortening (right) for case B (quadriaxial layup) with t = 24 mm and 3% imperfection amplitude.

7.7.3 Alternative Ply Region Sizes

Analyses with alternative ply region sizes have been performed to investigate whether this will affect the strength predictions. For the plate shown in Fig. 1, regions 1, 3, 7 and 9 are modified to 100 mm × 100 mm each, regions 2 and 8 are each 300 mm × 100 mm, regions 4 and 6 are 100 mm × 300 mm and region 5 is 300 mm × 300 mm. The ultimate strength predictions are provided in Table 4 for a selected number of cases. For a given imperfection amplitude, corresponding plate thickness (t) and number of plies (ply regions), the table shows the ultimate stresses (σ_{max}) from Section 7.7.1 and the present model. In the last column, these predictions have been compared to the ABAQUS results (σ_{max_ref}). Compared to ABAQUS, the ultimate strength predictions using the alternative ply region sizes are 1% - 2% higher than the predictions for the corresponding cases in Section 7.7.1. It is conceivable that a more drastic variation of the plate division might give greater differences. However, this has not been pursued in the present study.

Table 4
Strength predictions conducted by the alternative ply region sizes.

Layup case	Imp. % of *b*	*t* (mm)	No. of plies (no. of ply regions)	σ_{max} from Section 7.7.1 (MPa)	σ_{max} from alternative ply regions (MPa)	σ_{max_ref} (MPa)	$\sigma_{max}/\sigma_{max\_ref}$	
							σ_{max} from Section 7.7.1	σ_{max} from alternative ply regions
A1	1.0	10.02	34 (306)	109.77	111.26	130	0.84	0.86
A3	1.0	24.94	34 (306)	193.35	195.43	235	0.82	0.83
A5	1.0	49.98	34 (306)	399.82	405.52	435	0.92	0.93
B1	1.0	8.00	8 (72)	108.03	109.11	107	1.01	1.02
B3	1.0	24.00	24 (216)	195.89	197.90	210	0.93	0.94
B5	1.0	48.00	48 (432)	271.95	275.32	302	0.90	0.91

7.8 PRDM-DF2 with Linear Material Degradation

7.8.1 Ultimate Strength Predictions

The detailed results using PRDM-DF2 are provided in Appendix D, Tables D.3-D.4 for layup cases A and B, respectively. The results are presented graphically in Figs. 28-29 for case A layups and Figs. 30-31 for case B layups.

For case A layups, considering ultimate strengths, PRDM-DF2 provides higher predictions than PRDM-DF1. The greatest improvements obtained by using DF2 are found for layups A2 and A3. The PRDM-DF2 estimations are in the range 5% higher to 11% lower than ABAQUS results, i.e. the discrepancy suggested in Fig. 21 has been reduced drastically. Further, the linear degradation model provides higher strength estimations than the results implemented with the instantaneous degradation model given in Section 7.6. Figure 29 shows little sensitivity to geometric imperfections for *b*/*t* values greater than 25 from both the present model and the results from [10]. The elastic critical load curve is located lower than the corresponding strength predictions for *b*/*t* values greater than 19 for both the present model and the ABAQUS results.

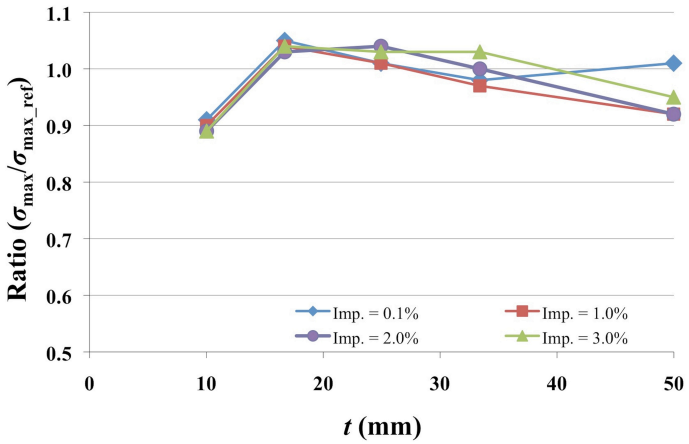

Fig. 28. Case A (triaxial) layups with ply region degradation model (DF2): the ultimate strengths from the present analyses are compared to the reference values σ_{max_ref} obtained by Misirlis, for various plate thicknesses *t* and imperfection amplitudes.

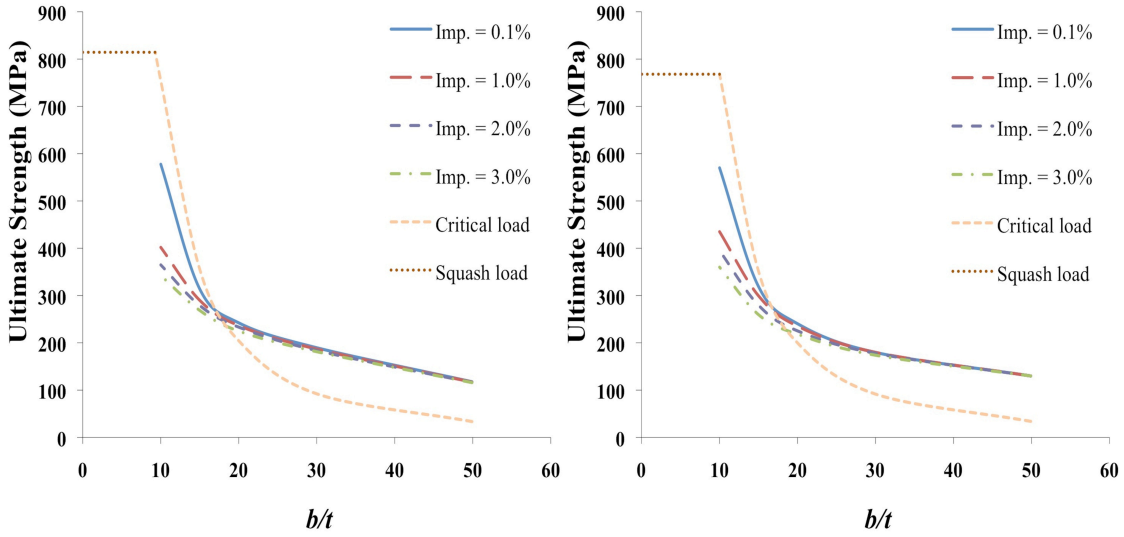

Fig. 29. Case A (triaxial layup) with ply region degradation model (DF2): the ultimate strengths from the present analyses (left) are compared to the corresponding results obtained by Misirlis (right), for various *b*/*t* values and imperfection amplitudes.

For layup case B, by applying DF2 and comparing to the results achieved by PRDM-DF1, the strength predictions have *decreased* for most of the layups except for layup B1 and layup B4 with 2% imperfection. Overall, the PRDM-DF2 estimations are in the range 5% higher to 17% lower than Misirlis's ABAQUS results. Again, a similar trend is observed to that for case A; higher ultimate strengths are predicted by using the linear material degradation model compared to the instantaneous material degradation model. Figure 31 shows that initial imperfections have very little effect on the strength predictions for *b*/*t* values greater than 30 and 25 for the present model and Misirlis's results, respectively. The ultimate strengths are significantly higher than the elastic critical loads for *b*/*t* values greater than 22-23 for both the present model and ABAQUS.

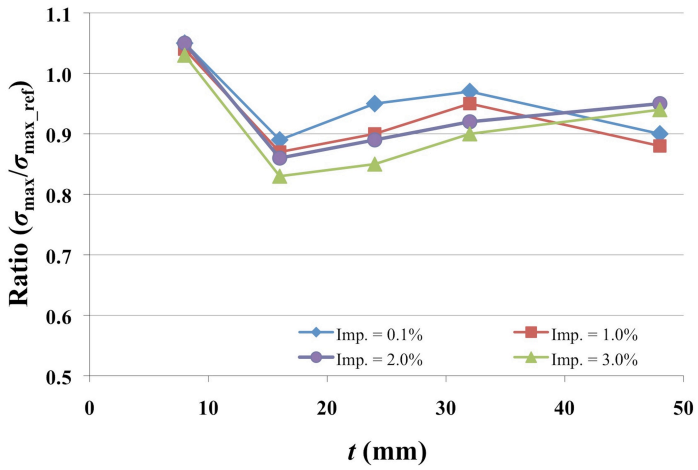

Fig. 30. Case B (quadriaxial) layups with ply region degradation model (DF2): the ultimate strengths from the present analyses are compared to the reference values σ_{max_ref} obtained by Misirlis, for various plate thicknesses *t* and imperfection amplitudes.

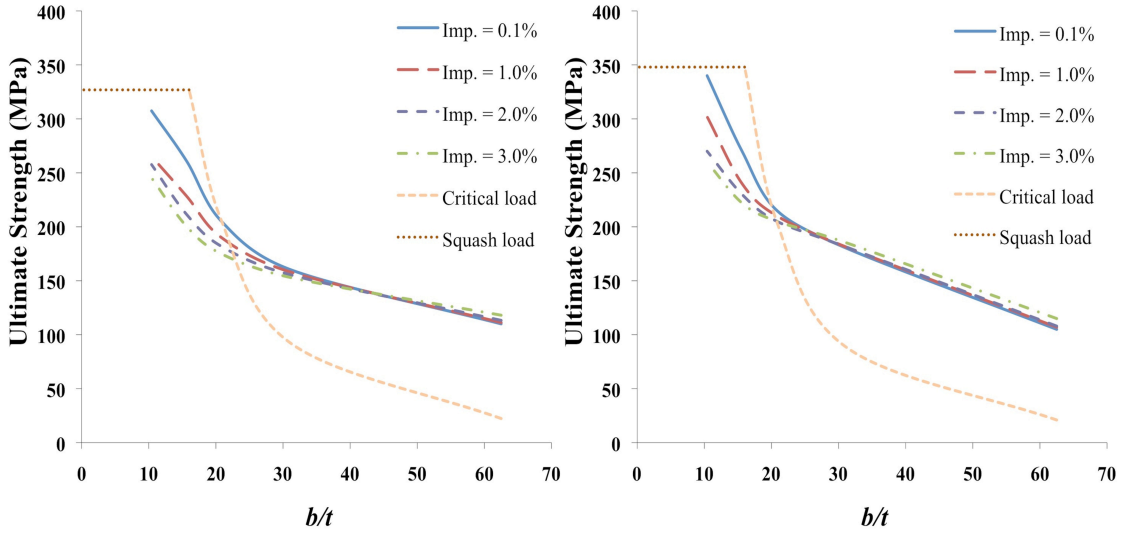

Fig. 31. Case B (quadriaxial layup) with ply region degradation model (DF2): the ultimate strengths from the present analyses (left) are compared to the corresponding results obtained by Misirlis (right), for various *b*/*t* values and imperfection amplitudes.

7.8.2 Alternative Material Degradation for Fibre Failure

For both matrix and fibre failure modes, a linear material degradation has been considered in the previous sections and in ABAQUS. In reality, the material stiffness associated with the fibre failure modes degrades more steeply than for matrix failure modes. In order to give a more realistic picture of the material degradation, the ultimate strength analysis has been performed with $\delta^{f}_{eq,\,\text{fibre}} = 1.1\delta^{0}_{eq,\,\text{fibre}}$ associated with the fibre failure modes and $\delta^{f}_{eq,\,\text{matrix}} = 2\delta^{0}_{eq,\,\text{matrix}}$ associated with the matrix failure modes. The results are provided in Table 5 for a limited number of cases. For a given imperfection amplitude, corresponding plate thickness (t) and number of plies (and ply regions), the table shows the ultimate stresses ($\sigma_{\text{max\_ref}}$) from Section 7.8.1 and the present model. These are further compared to the results from ABAQUS in the last column. Compared to ABAQUS, the ultimate strengths produced by the alternative material degradation are in the range of 1% - 6% lower than the estimations for the corresponding cases in Section 7.8.1.

Table 5
Strength predictions conducted by the alternative material degradation due to fibre failure.

Layup case	Imp. % of *b*	*t* (mm)	No. of plies (no. of ply regions)	σ_{max} from Section 7.8.1 (MPa)	σ_{max} from alternative mater. deg. (MPa)	$\sigma_{\text{max\_ref}}$ (MPa)	$\sigma_{\text{max}}/\sigma_{\text{max\_ref}}$	
							σ_{max} from Section 7.8.1	σ_{max} from alternative mater. deg.
A3	3.0	24.94	34 (306)	224.60	210.40	235	1.03	0.97
A5	1.0	49.98	34 (306)	401.84	382.96	435	0.92	0.88
B1	3.0	8.00	8 (72)	118.09	117.26	107	1.03	1.02
B3	1.0	24.00	24 (216)	190.01	180.91	210	0.90	0.86

7.9 Alternative Layup Configurations

Other layup configurations have been considered in this section. It is interesting to analyse a more balanced triaxial layup (case C) and a more unbalanced quadriaxial layup (case D):

- Case C, a triaxial layup: $[-45/+45/0]_{4S}$
- Case D, a quasi-isotropic, quadriaxial layup: $[0_3/+45/90/-45]_{2S}$

The material properties are given in Table 1, and the plate thicknesses for cases C and D are given in Tables 6-7. The plate size and the imperfection shape are similar to those given in Section 7.1. Note that only the maximum initial imperfection amplitude with 0.1% of the width b has been investigated in this section. The analyses have been performed with PRDM-DF1 and PRDM-DF2 implemented with the linear material degradation model. The results have been compared to the nonlinear FE analysis conducted for these layups by Braaten and Boström [25] in cooperation with DNV GL, using ABAQUS.

Table 6
Plate thicknesses and ply thicknesses for case C.

Layup case	b/t	t (mm)	t_0, $t_{\pm45}$, t_{90} (mm)
C1	50	10.00	0.42
C2	30	16.70	0.70
C3	20	25.00	1.04
C4	15	33.30	1.39
C5	10	50.00	2.08

Table 7
Plate thicknesses and ply thicknesses for case D.

Layup case	b/t	t (mm)	t_0 (mm)	$t_{\pm45}$, t_{90} (mm)
D1	50	10.00	0.52	0.31
D2	30	16.70	0.87	0.52
D3	20	25.00	1.30	0.78
D4	15	33.30	1.73	1.04
D5	10	50.00	2.61	1.56

The ultimate strengths predicted using PRDM-DF1 for layup cases C and D are provided in Table D.5 in Appendix D. The ratios of the ultimate strengths estimated using the present model to the reference values found by Braaten and Boström (σ_{max_ref2}) are shown in Fig. 32 for various values of plate thickness t. For case C layups, the predictions are highly satisfactory in that they range from 2% higher to 8% lower than the ABAQUS analysis. For case D layups, the ultimate strength estimations are in the range 5% higher to 31% lower than the ABAQUS results. The greatest deviation is found for a moderately thick plate (D3) for which the strength predicted is even lower than the prediction for a thinner plate (D2).

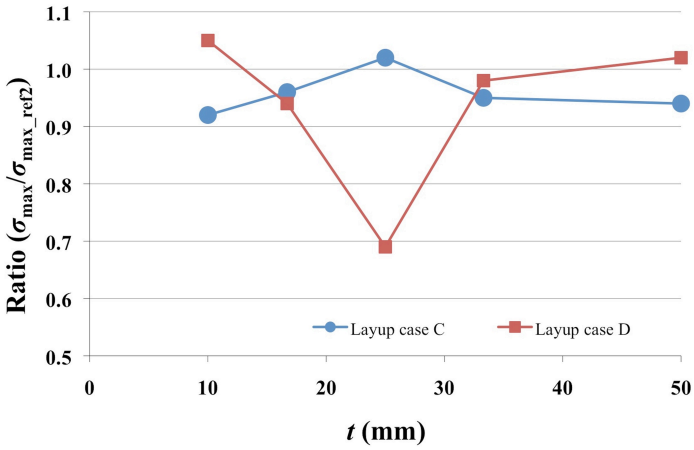

Fig. 32. Layup cases C (triaxial) and D (quadriaxial) with ply region degradation model (DF1): the ultimate strengths from the present analyses are compared to the reference values σ_{max_ref2} obtained by Braaten and Boström [25], for various plate thicknesses t and imperfection amplitude 0.1% of the width.

The corresponding results using PRDM-DF2 for layup cases C and D are given in Fig. 33 and Table D.6 in Appendix D. The ultimate strength predictions achieved for case C layups are 0% - 20% lower than the ABAQUS results. The greatest deviations are found for layups C1 and C2, while the results for the remaining cases are almost unchanged compared to the corresponding cases with DF1. The strength estimations obtained for case D layups are in the range 5% lower to 24% higher than ABAQUS predictions. The discrepancy that existed for layup D3 using PRDM-DF1 has been reduced significantly, and this is currently 5% lower than the ABAQUS result. A special case has been observed: for layup D1, the prediction is 24% higher than ABAQUS analysis. The reason for this rather surprising outcome is unclear. However, inspection of the results from [25] suggests an error in the tabulated ABAQUS result for this particular case.

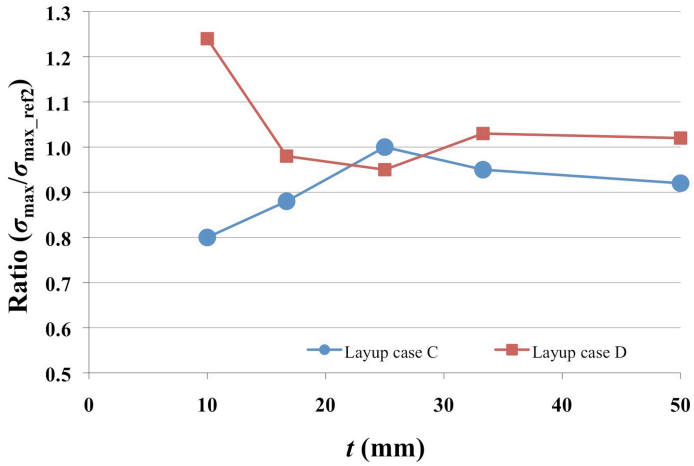

Fig. 33. Layup cases C (triaxial) and D (quadriaxial) with ply region degradation model (DF2): the ultimate strengths from the present analyses are compared to the reference values σ_{max_ref2} obtained by Braaten and Boström, for various plate thicknesses t and imperfection amplitude 0.1% of the width.

8 DISCUSSION

8.1 CPDM and PRDM

In the first degradation approach, CPDM, fulfilment of the failure criterion at any position in a ply leads to instantaneous degradation of corresponding stiffness properties throughout that ply. In the slightly more detailed approach, PRDM-DF1, the plate is divided into nine regions and the stiffness degradation is limited to the affected regions of a failed ply.

For the triaxial layup configuration, case A, the predicted ultimate stresses using CPDM are 14% - 33% smaller than those of Misirlis, while the deviations are in the range of 14% - 29% by using PRDM-DF1. The greatest improvements, 7% - 9%, between the predictions using CPDM and PRDM-DFI are observed for thin plates (A1). However, the improvements obtained are simply 0% - 2% for moderately thick (A3) and thick plates (A5).

For the quadriaxial layup, case B, the ultimate strength predictions using CPDM produced a more stable deviation in the range of 11% - 21% compared to Misirlis's ABAQUS results, while the differences are in the range of 3% - 19% by using PRDM-DF1. The greatest improvements, 7% - 11%, between the predictions using CPDM and PRDM-DFI are observed for thin plates (B1). For moderately thick (B3) and thick plates (B5), the improvements obtained are 0% - 4%.

The analyses with PRDM-DFI thus provide better estimates than those with CPDM for many of the cases. Especially for thin plates, characterised by small ply thicknesses (case A) and few plies (case B), PRDM-DFI gives appreciably better results. Ply region based material degradation results in smaller stiffness-reduced areas compared to entire ply based material degradation. The total plate stiffness can thus be significantly larger for these plates, even with a small number of regions undamaged. However, for moderately thick and thick plates the improvements obtained are either negligible or quite small for both layup cases. This could be explained by the fact that many plies and ply regions have to fail before the ultimate strength is reached. The few ply regions left with intact material properties are unlikely to affect the total plate stiffness significantly, since thicker plates have more plies and/or greater ply thicknesses. These effects are closely related to the fact that thick plates undergo less bending deformation than thinner plates, so that stresses are more uniformly distributed throughout the plate.

An alternative set of ply region sizes were investigated in Section 7.7.3. Considering the ultimate strength estimations, no clear trend has been detected compared to the original ply region sizes.

8.2 Instantaneous and Linear Degradation of Materials

Damage initiation refers to the onset of stiffness reduction, and the corresponding material properties are either degraded directly to a predefined value or a linear material degradation model is applied.

Considering case A layups using PRDM-DF1 and PRDM-DF2, the linear degradation model gives higher ultimate strength predictions than the results produced by the instantaneous degradation model for all cases except one. When using DF1, the greatest improvements by using linear degradation, 6% - 20%, are found for layup A5. The differences are in the range from 2% lower to 11% higher for layup A3 and 3% - 9% higher for layup A1. The 2% lower prediction occurred for layup A3 with 0.1% imperfection. The reason for this exceptional outcome is unclear. When using linear degradation with DF2, the predictions have been improved by 6% - 21%, compared with instantaneous degradation, for layup A5, and by 6% - 8% and 8% - 9% for layups A3 and A1, respectively.

For case B layups using both PRDM-DF1 and PRDM-DF2, the ultimate strength predictions achieved by the linear degradation model are higher than the estimations implemented with the instantaneous degradation model. Considering DF1, the improvement is 6% for layup B1. For layups B3 and B5, the improvements are 8% - 13% and 1% - 15%, respectively. Considering DF2, the improvements obtained are 2% - 3% for layup B1, and by 10% - 15% and 1% - 18% for layups B3 and B5, respectively.

Implementation with the linear degradation model brings the strength predictions closer to those conducted by Misirlis. The greatest improvements are generally obtained for thick and moderately thick plates for both layup cases. This could be explained by the fact that the linear degradation model leads to smoother stiffness reduction in which the post-damage behaviour of the materials is based on the stress-displacement relation in a ply region. As mentioned in the previous section, thicker plates undergo less bending deformation, so that stresses and displacements evolve more gradually throughout the plate. Instantaneous degradation of the material properties causes an unnecessarily large reduction of the plate stiffness, and in turn lower ultimate strengths are predicted. On the other hand, thin plates undergo more bending deformation, so that the damage spreads much faster throughout the plate, thus the instantaneous degradation model will provide a fairly correct picture of the material failure propagation. Another important disadvantage by using the instantaneous degradation model is the time-consuming performance in terms of the unloading and reloading procedure (see Section 5.3.2).

In association with the fibre failure modes, an alternative material degradation has been suggested in Section 7.8.2 in which the corresponding material properties are reduced more instantaneously, while the matrix failure modes still use the linear degradation model. This modification gives a more realistic picture of the damage development. In the analysis with ABAQUS, which only allows using the same α value for all failure modes, Misirlis has applied a value ($\alpha = 2$) that is appropriate for matrix failure. Compared to results in [10], the strengths predicted using PRDM-DF2 are 1% - 6% lower than those produced by PRDM-DF2 with the unmodified linear degradation model.

8.3 DF1 and DF2

Two alternative in-plane displacement fields have been investigated. In DF1, no movements are allowed along the four edges for displacement components u_0 and v_0 apart from the linear components. In DF2, u_0 is permitted to vary more freely along the edges $y = 0,b$ and v_0 is permitted to vary more freely along the edges $x = 0,a$. However, while DF1 gives a symmetric variation across the plate, DF2 gives an antisymmetric variation.

For the triaxial layup configuration, case A, the predicted ultimate stresses using PRDM-DF1 and linear degradation model are 0% - 26% smaller than those from ABAQUS. The differences are in the range 5% higher to 11% lower by using PRDM-DF2, i.e. a clear improvement is achieved, especially for layups A2 and A3. The same trend is observed for these models implemented with the instantaneous material degradation; the greatest improvements are obtained for a moderately thick plate, while the differences are almost negligible for a thick plate.

For the quadriaxial layup configuration, case B, the PRDM-DF1 estimations using the linear degradation model are in the range 3% higher to 15% lower than Misirlis's ABAQUS results. Using PRDM-DF2, the differences become 5% higher to 17% lower. Compared to DF1, the strength predictions with DF2 have *decreased* for most of the cases except for layup B1 and layup B4 with 2% imperfection. The same trend is found for both PRDMs implemented with the instantaneous material degradation model.

DF1 seems to give best predictions for balanced layup cases, while DF2 is better for unbalanced layup cases. This statement has been strengthened by investigating two more layup configurations, cases C and D in Section 7.9. Reddy primarily suggested DF2 for anti-symmetric laminates. All cases investigated in Section 7 are initially symmetric, i.e. up to first ply failure DF1 will give the most correct displacement responses. Considering ultimate stresses, it seems that failure sequence, layup configuration and plate thickness are all factors that will influence the choice of DF1 or DF2:

1. The failure usually initiates on the convex side (outermost 0° plies) of the plate for most of the cases investigated. The matrix failure will propagate on this side of the plate to a certain point before the damage initiates on the concave side. At this point, the material degradation causes the layup to become fairly asymmetric, and this asymmetry will normally be maintained throughout the degradation procedure. Since DF2 is intended for anti-symmetric laminates, this displacement field will provide more correct displacement responses.

2. The unbalanced layup cases A and D are most affected: the 0° plies that undergo matrix failure as described in 1) have greater ply thickness than the remaining plies (±45° and 90°). This will increase the asymmetry that already exists in the laminate.

3. For thick plates, the displacement responses are more stable due to their larger ply thicknesses and stiffness, and in turn the failure spreads more gradually

throughout the plate. After damage initiation, the material properties degraded on the convex/concave side of the plate are unlikely to influence the symmetry significantly before the failure initiates on the other side of the plate. Thus, DF1 and DF2 provide more or less equivalent displacement responses.

9 CONCLUSIONS

Ultimate strength prediction using a semi-analytical method has been established for simply supported composite plates under uniaxial in-plane compression. The present model is able to take account of post-buckling behaviour, out-of-plane shear deformation and initial geometric imperfections. Two different area-based degradation approaches have been proposed, where the stiffness reduction has been either applied to the entire failed ply or to the affected region of a ply. Further, linear degradation of the material properties has been compared to the instantaneous material degradation. Two alternatives of displacement fields have been studied for their influence on the strength estimations. A parametric study has been performed for square plates with a range of thicknesses, initial imperfections. Four different types of composite layup have been considered. The numerical results have been compared with reference values obtained using advanced FE analysis by Misirlis [10]. Based on that evaluation, the recommended model for further ultimate strength predictions is PRDM-DF2 combined with the linear material degradation model. It is clear from the investigation that the ultimate strengths are much higher than the elastic critical loads, especially for thin plates. Indication of sensitivity to geometric imperfections is detected for b/t ratio less than 25-30. As mentioned by Brubak et al. [2,3], similar analysis methods applied to stiffened steel plates have been implemented in the computerised software code PULS for use in the strength assessment of steel ship structures (see Steen et al. [26]). The analysis methods developed in the current work will enable this software to be adapted in the near future to include laminated composites.

ACKNOWLEDGEMENTS

The author wishes to thank Professor Brian Hayman at the University of Oslo for his constructive guidance and valuable discussions during the development of this research work. Thanks are also due to Professor Jostein Hellesland at the University of Oslo for his valuable suggestions and useful critiques, and to Lars Brubak, Associate Professor at the university of Oslo and Senior Engineer at the Det Norske Veritas Germanischer Lloyd (DNV GL), for his support and advice.

REFERENCES

[1] Steen E. Application of the perturbation method to plate buckling problems. Research Report in Mechanics No. 98-1. Norway: University of Oslo; 1998.

[2] Brubak L, Hellesland J, Steen E. Semi-analytical buckling strength analysis of plates with arbitrary stiffener arrangements. J Constr Steel Res 2007;63(4):532-543.

[3] Brubak L, Hellesland J. Approximate buckling strength analysis of arbitrarily stiffened, stepped plates. Eng Struct 2007;29(9):2321-2333.

[4] Brubak L, Hellesland J. Semi-analytical postbuckling and strength analysis of arbitrarily stiffened plates in local and global bending. Thin-Walled Struct 2007;45(6):620-633.

[5] Brubak L, Hellesland J. Strength criteria in semi-analytical, large deflection analysis of stiffened plates in local and global bending, Thin-walled Struct 2008;46(12):1382-1390.

[6] Brubak L, Hellesland J. Semi-analytical postbuckling analysis of stiffened imperfect plates with a free or stiffened edge. Comput Struct 2011;89(17-18):1574-1585.

[7] Yang QJ, Hayman B, Osnes H. Trials with a simplified method for buckling and ultimate strength analysis of composite plates. Research Report in Mechanics No. 2012-1. Norway: University of Oslo; 2012.

[8] Yang QJ, Hayman B, Osnes H. Simplified buckling and ultimate strength analysis of composite plates in compression. Compos Part B 2013;54:343-352.

[9] Hashin Z, Rotem A. A fatigue failure criterion for fiber reinforced materials. J Compos Mater 1973;7:448-464.

[10] Hayman B, Berggreen C, Lundsgaard-Larsen C, Delarche A, Toftegaard H, Dow RS, Downes J, Misirlis K, Tsouvalis N, Douka C. Studies of the buckling of composite plates in compression. Ships Offshore Struct 2011;6(1-2):81-92.

[11] Reddy JN. Mechanics of laminated composite plates and shells. 2nd ed. USA: CRC Press; 2004.

[12] Marguerre K. Zur Theorie der gekrümmten platte grosser formänderung. In: Proceedings of the 5th International Congress for Applied Mechanics. Cambridge: USA; 1938, p. 93-101.

[13] Agarwal BD, Broutman LJ, Chandrashekhara K. Analysis and performance of fiber composites. 3rd ed. USA: Wiley; 2006.

[14] Bažant ZP, Cedolin L. Stability of structures. USA: Oxford University Press; 1991.

[15] Byklum E. Ultimate strength analysis of stiffened steel and aluminium panels using semi-analytical methods. Dr. Ing. Thesis. Norway: Norwegian University of Science and Technology; 2002.

[16] Riks E. An incremental approach to the solution of snapping and buckling problems. Int J Solids Struct 1979;15:529-551.

[17] Wempner GA. Discrete approximations related to nonlinear theories of solids. Int J Solids Struct 1971;7:1581-1599.

[18] Chen WF, Lui EM. Stability design of steel frames. USA: CRC Press; 1991.

[19] Crisfield MA. Non-linear finite element analysis of solids and structures. Vol. 1. England: Wiley; 1991.

[20] Kang YJ. Nonlinear geometric, material and time dependent analysis of reinforced and prestressed concrete frames. Report No. UC SESM 77-1. USA: College of Engineering, University of California, Berkeley; 1977.

[21] Matzenmiller A, Lubliner J, Taylor RL. A constitutive model for anisotropic damage in fiber-composites. Mech Mater 1995;20(2):125-152.

[22] Offshore standard DNV-OS-C501 Composite components. Norway: Det Norske Veritas; 2003.

[23] Abaqus Documentation. Version 6.11. USA: Dassault Systèms Simulia Corporation; 2011.

[24] Misirlis K. Progressive collapse analysis of composite ship hull sections. PhD Thesis. Newcastle: Newcastle University; 2012.

[25] Braaten E, Boström J. Ultimate strength study of composite plates. Master's Thesis. Göteborg: Chalmers University of Technology; 2013.

[26] Steen E, Byklum E, Vilming KG, Østvold TK. Computerized buckling models for ultimate strength assessments of stiffened ship hull panels. In: Proceedings of the 9th International Symposium on Practical Design of Ships and Other Floating Structures. Germany; 2004, p. 235-242.

APPENDIX A: DAMAGE EVOLUTION AND FAILURE MODES

Equivalent displacement (σ_{eq}) and stress (δ_{eq}) for each of the four damage modes are defined as follows:

- Fibre tension:

$$\delta_{eq}^{ft} = \langle \varepsilon_{11} \rangle \tag{A.1a}$$

$$\sigma_{eq}^{ft} = \frac{\langle \sigma_{11} \rangle \langle \varepsilon_{11} \rangle}{\delta_{eq}^{ft}} = \langle \sigma_{11} \rangle \tag{A.1b}$$

- Fibre compression:

$$\delta_{eq}^{fc} = \langle -\varepsilon_{11} \rangle \tag{A.2a}$$

$$\sigma_{eq}^{fc} = \frac{\langle -\sigma_{11} \rangle \langle -\varepsilon_{11} \rangle}{\delta_{eq}^{fc}} = \langle -\sigma_{11} \rangle \tag{A.2b}$$

- Matrix tension:

$$\delta_{eq}^{mt} = \sqrt{\langle \varepsilon_{22} \rangle^2 + \gamma_{12}^2} \tag{A.3a}$$

$$\sigma_{eq}^{mt} = \frac{\langle \sigma_{22} \rangle \langle \varepsilon_{22} \rangle + \tau_{12}\gamma_{12}}{\delta_{eq}^{mt}} \tag{A.3b}$$

- Matrix compression:

$$\delta_{eq}^{mc} = \sqrt{\langle -\varepsilon_{22} \rangle^2 + \gamma_{12}^2} \tag{A.4a}$$

$$\sigma_{eq}^{mc} = \frac{\langle -\sigma_{22} \rangle \langle -\varepsilon_{22} \rangle + \tau_{12}\gamma_{12}}{\delta_{eq}^{mc}} \tag{A.4b}$$

The symbol $\langle\ \rangle$ in the equations above represents the Macaulay bracket operator which is defined for every $a \in \Re$ as $\langle a \rangle = (a + |a|)/2$.

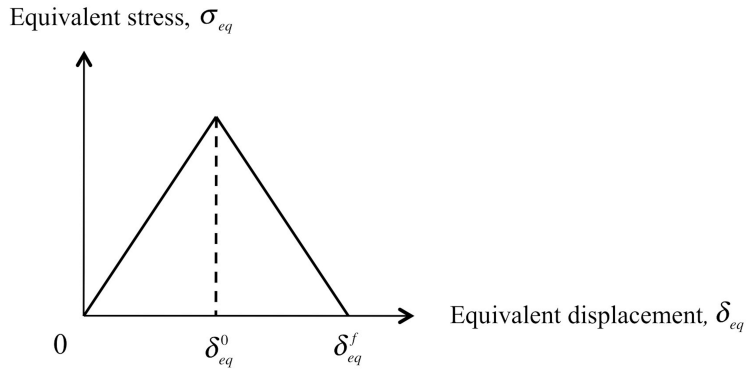

Fig. A.1. Linear damage evolution.

Computation of the damage variables is based on the stress-displacement relation shown in Fig. A.1. The positive slope of the stress-displacement curve prior to damage initiation corresponds to linear elastic material behaviour. After damage initiation, the negative slope is achieved by evolution of the respective damage variables according to the equations (A.1)-(A.4). After damage initiation (i.e. $\delta_{eq} \geq \delta_{eq}^{0}$), the damage variable d_i for a particular mode is achieved by:

$$d_i = \frac{\delta_{eq}^{f}\left(\delta_{eq} - \delta_{eq}^{0}\right)}{\delta_{eq}\left(\delta_{eq}^{f} - \delta_{eq}^{0}\right)} \tag{A.5}$$

APPENDIX B: COVERGENCE TEST

In Tables B.1-B.3, for a given initial geometric imperfection amplitude and plate thickness (t), the number of terms included are shown alongside the strength estimations using the present method (σ_{max}) and these have been compared to the results provided by Misirlis (σ_{max_ref}). Further, 47 terms corresponds to $N = M = 3$, 127 terms corresponds to $N = M = 5$, 247 terms to $N = M = 7$ and 407 terms to $N = M = 9$, 607 terms corresponds to $N = M = 11$.

Table B.1
The ultimate strengths for case A using CPDM.

Imp. % of b	Plate thickness, t (mm)	Number of terms	σ_{max} (MPa)	σ_{max_ref} (MPa)	$\sigma_{max}/\sigma_{max\_ref}$
0.1	10.02	47	133.85	130	1.03
		127	105.76	130	0.81
		249	97.50	130	0.75
		407	94.94	130	0.73
		607	94.22	130	0.72
3.0	10.02	127	101.89	130	0.78
		249	91.40	130	0.70
		407	87.73	130	0.67
		607	86.65	130	0.67
1.0	24.94	47	177.17	235	0.75
		127	171.40	235	0.73
		249	170.65	235	0.73
		407	170.16	235	0.72

3.0	24.94	47	159.51	218	0.73
		127	149.98	218	0.69
		249	148.49	218	0.68
1.0	49.98	47	376.88	435	0.87
		127	374.88	435	0.86

Table B.2
The ultimate strengths for case B using CPDM.

Imp. % of b	Plate thickness, t (mm)	Number of terms	σ_{max} (MPa)	σ_{max_ref} (MPa)	$\sigma_{max}/\sigma_{max\_ref}$
1.0	8	127	111.27	107	1.04
		249	96.75	107	0.90
		407	91.51	107	0.86
		607	90.87	107	0.85
1.0	24	47	175.64	210	0.84
		127	174.05	210	0.83
		249	171.48	210	0.82
		407	169.42	210	0.81
0.1	48	127	301.97	340	0.89
		249	301.97	340	0.89
3.0	48	47	212.28	260	0.82
		127	210.72	260	0.81
		249	211.24	260	0.81

Table B.3
The ultimate strengths for case A using PRDM-DF1.

Imp. % of b	Plate thickness, t (mm)	Number of terms	σ_{max} (MPa)	σ_{max_ref} (MPa)	$\sigma_{max}/\sigma_{max\_ref}$
3.0	24.94	127	162.27	218	0.74
		249	155.30	218	0.71
		407	154.80	218	0.71
3.0	49.98	127	299.73	360	0.83
		249	302.73	360	0.84

APPENDIX C: TABULATED RESULTS - INSTANTANEOUS MATERIAL DEGRADATION

For a given initial geometric imperfection amplitude, plate thickness (t) and total number of plies (ply regions), Tables C.1-C.6 show the total number of terms included, the calculated stress (σ_{FPF}) at first ply failure (FPF), and location of first ply in terms of ply number and direction of that ply. By investigating a last ply failure condition ("LPF"), the ultimate stress (σ_{max}) using the semi-analytical method is presented, and the number of plies (ply regions) that have failed at this stage is also provided. Further, the ply in which this last ply failure occurs (as ply number and direction) is shown for CPDM. The results from the analysis are compared with those conducted by Misirlis (σ_{max_ref}). The ratio of the ultimate strength from the present model to that found by Misirlis are given in the last column ($\sigma_{max}/\sigma_{max\_ref}$).

The numbers of terms used are shown in Tables C.1-C.6; 127 terms corresponds to $N = M = 5$, 247 terms to $N = M = 7$ and 407 terms to $N = M = 9$. For case B1 and for case A1 with displacement field 2, $\Delta\eta = 0.01$ has been used. The remaining layup cases, $\Delta\eta$ is set to 0.10. The chosen basic values of N_x are 150 N/mm and 200 N/mm for layups A1 and B1, respectively. For layups A3 and B3, N_x is set to 500 N/mm. The remaining layups are implemented with $N_x = 2000$ N/mm.

Table C.1
Complete ply degradation model for Case A (triaxial layup).

				FPF		"LPF"				
Imp. % of *b*	*t* (mm)	No. of plies	No. of terms	σ_{FPF} (MPa)	Ply no. (direction)	σ_{max} (MPa)	No. of matrix (fibre) failed plies	Ply no. (direction)	σ_{max_ref} (MPa)	$\frac{\sigma_{max}}{\sigma_{max\_ref}}$
0.1	10.02	34	407	39.86	32 (0°)	94.94	34 (1)	34 (-45°)	130	0.73
0.1	24.94	34	127	172.00	32 (0°)	186.66	34 (1)	34 (-45°)	240	0.78
0.1	49.98	34	127	382.13	1 (-45°)	453.24	34 (1)	3 (0°)	570	0.80
1.0	10.02	34	407	31.64	32 (0°)	90.92	34 (1)	34 (-45°)	130	0.70
1.0	24.94	34	127	71.64	32 (0°)	171.40	34 (1)	34 (-45°)	235	0.73
1.0	49.98	34	127	149.55	32 (0°)	374.88	34 (1)	3 (0°)	435	0.86
3.0	10.02	34	407	22.96	32 (0°)	87.73	34 (1)	34 (-45°)	130	0.67
3.0	24.94	34	127	39.05	32 (0°)	149.98	34 (1)	34 (-45°)	218	0.69
3.0	49.98	34	127	64.26	32 (0°)	292.84	34 (1)	34 (-45°)	360	0.81

Table C.2
Complete ply degradation model for Case B (quadriaxial layup).

				FPF		"LPF"				
Imp. % of *b*	*t* (mm)	No. of plies	No. of terms	σ_{FPF} (MPa)	Ply no. (direction)	σ_{max} (MPa)	No. of matrix (fibre) failed plies	Ply no. (direction)	σ_{max_ref} (MPa)	$\frac{\sigma_{max}}{\sigma_{max\_ref}}$
0.1	8.00	8	407	29.08	8 (0°)	89.85	8 (1)	7 (45°)	105	0.86
0.1	24.00	24	247	170.92	24 (0°)	177.66	24 (1)	1 (0°)	215	0.83
0.1	48.00	48	127	204.13	3 (90°)	301.97	36 (1*)	1 (0°)	340	0.89
1.0	8.00	8	407	27.38	8 (0°)	91.51	8 (2)	2 (45°)	107	0.86
1.0	24.00	24	247	69.49	24 (0°)	171.48	24 (1)	23 (45°)	210	0.82
1.0	48.00	48	127	144.77	48 (0°)	250.92	42 (1*)	1 (0°)	302	0.83
3.0	8.00	8	407	26.08	8 (0°)	94.11	8 (1)	7 (45°)	115	0.82
3.0	24.00	24	247	35.62	24 (0°)	162.77	24 (2)	2 (45°)	205	0.79
3.0	48.00	48	247	61.70	48 (0°)	211.24	48 (1)	1 (0°)	260	0.81

Table C.3
Ply region degradation model (PRDM-DF1) for Case A (triaxial layup).

Imp. % of *b*	*t* (mm)	No. of plies (no. of ply regions)	No. of terms	FPF		"LPF"				
				σ_{FPF} (MPa)	Ply no. (direction)	σ_{max} (MPa)	No. of matrix failed ply regions	No. of fibre failed ply regions	σ_{max_ref} (MPa)	$\frac{\sigma_{max}}{\sigma_{max\_ref}}$
0.1	10.02	34 (306)	407	39.86	32 (0°)	106.24	277	9	130	0.82
0.1	24.94	34 (306)	127	172.00	32 (0°)	186.68	293	2	240	0.78
0.1	49.98	34 (306)	127	382.13	1 (-45°)	453.24	306	1	570	0.80
1.0	10.02	34 (306)	407	31.64	32 (0°)	99.57	302	18	130	0.77
1.0	24.94	34 (306)	247	71.39	32 (0°)	175.34	276	12	235	0.75
1.0	49.98	34 (306)	127	149.55	32 (0°)	375.89	301	1*	435	0.86
3.0	10.02	34 (306)	407	22.96	32 (0°)	96.03	303	18	130	0.74
3.0	24.94	34 (306)	247	38.92	32 (0°)	155.30	276	10	218	0.71
3.0	49.98	34 (306)	127	64.26	32 (0°)	299.73	301	14	360	0.83

*In these ply regions fibre failure occurred without matrix failure.

Table C.4
Ply region degradation model (PRDM-DF1) for Case B (quadriaxial layup).

Imp. % of *b*	*t* (mm)	No. of plies (no. of ply regions)	No. of terms	FPF		"LPF"				
				σ_{FPF} (MPa)	Ply no. (direction)	σ_{max} (MPa)	No. of matrix failed ply regions	No. of fibre failed ply regions	σ_{max_ref} (MPa)	$\frac{\sigma_{max}}{\sigma_{max\_ref}}$
0.1	8.00	8 (72)	407	29.08	8 (0°)	101.71	57	4	105	0.97
0.1	24.00	24 (216)	247	170.92	24 (0°)	178.32	209	1	215	0.83
0.1	48.00	48 (432)	247	204.13	3 (90°)	301.97	324	1*	340	0.89
1.0	8.00	8 (72)	407	27.38	8 (0°)	101.54	56	4	107	0.95
1.0	24.00	24 (216)	247	69.49	24 (0°)	177.05	208	4	210	0.84
1.0	48.00	48 (432)	247	144.77	48 (0°)	250.92	378	1*	302	0.83
3.0	8.00	8 (72)	407	26.08	8 (0°)	101.86	54	4	115	0.89
3.0	24.00	24 (216)	247	35.62	24 (0°)	170.62	202	6	205	0.83
3.0	48.00	48 (432)	247	61.70	48 (0°)	209.70	392	1*	260	0.81

*In these ply regions fibre failure occurred without matrix failure.

Table C.5
Ply region degradation model (PRDM-DF2) for Case A (triaxial layup).

Imp. % of *b*	*t* (mm)	No. of plies (no. of ply regions)	No. of terms	FPF		"LPF"				
				σ_{FPF} (MPa)	Ply no. (direction)	σ_{max} (MPa)	No. of matrix failed ply regions	No. of fibre failed ply regions	σ_{max_ref} (MPa)	$\frac{\sigma_{max}}{\sigma_{max\_ref}}$
0.1	10.02	34 (306)	407	42.50	32 (0°)	106.70	279	2	130	0.82
0.1	24.94	34 (306)	127	173.39	32 (0°)	224.13	295	1*	240	0.93
0.1	49.98	34 (306)	127	382.14	1 (-45°)	457.81	306	1	570	0.80

1.0	10.02	34 (306)	407	40.37	32 (0°)	106.16	283	2	130	0.82
1.0	24.94	34 (306)	247	77.65	32 (0°)	219.19	278	1*	235	0.93
1.0	49.98	34 (306)	127	155.05	32 (0°)	372.95	301	1*	435	0.86
3.0	10.02	34 (306)	407	38.08	32 (0°)	105.55	284	2	130	0.81
3.0	24.94	34 (306)	247	49.57	32 (0°)	210.92	271	1*	218	0.97
3.0	49.98	34 (306)	127	73.02	32 (0°)	305.90	300	1*	360	0.85

*In these ply regions fibre failure occurred without matrix failure.

Table C.6
Ply region degradation model (PRDM-DF2) for Case B (quadriaxial layup).

				FPF		"LPF"				
Imp. % of b	t (mm)	No. of plies (no. of ply regions)	No. of terms	σ_{FPF} (MPa)	Ply no. (direction)	σ_{max} (MPa)	No. of matrix failed ply regions	No. of fibre failed ply regions	σ_{max_ref} (MPa)	$\frac{\sigma_{max}}{\sigma_{max\_ref}}$
0.1	8.00	8 (72)	407	32.47	8 (0°)	107.34	68	4	105	1.02
0.1	24.00	24 (216)	247	171.83	24 (0°)	171.93	1	0	215	0.80
0.1	48.00	48 (432)	247	204.13	3 (90°)	301.97	325	6*	340	0.89
1.0	8.00	8 (72)	407	32.15	8 (0°)	109.08	68	4	107	1.02
1.0	24.00	24 (216)	247	74.17	24 (0°)	165.21	204	3	210	0.79
1.0	48.00	48 (432)	247	148.93	48 (0°)	247.79	372	1*	302	0.82
3.0	8.00	8 (72)	407	36.24	8 (0°)	114.68	68	4	115	1.00
3.0	24.00	24 (216)	247	42.13	24 (0°)	154.48	199	2	205	0.75
3.0	48.00	48 (432)	247	68.47	48 (0°)	197.73	412	1*	260	0.76

*In these ply regions fibre failure occurred without matrix failure.

APPENDIX D: TABULATED RESULTS - LINEAR MATERIAL DEGRADATION

For a given initial geometric imperfection amplitude, plate thickness (t) and total number of plies (ply regions), Tables D.1-D.4 show the total number of terms included, the $\Delta\eta$ values and the calculated stress (σ_{FPF}) at first ply failure (FPF). The ultimate stress using the semi-analytical method is presented as σ_{max}. The results from the analysis are compared with those conducted by Misirlis (σ_{max_ref}). The ratio of the ultimate strength from the present model to that found by Misirlis are given in the last column ($\sigma_{max}/\sigma_{max\_ref}$). In Tables D.5-D.6, some changes have been made from Tables D.1-D.4. In addition to the information mentioned above, these tables provide also the chosen basic value of N_x and σ_{FPF} has been omitted. The ultimate stresses from the semi-analytical method have been compared with the ABAQUS results conducted by Braaten and Boström (σ_{max_ref2}).

The numbers of terms used are shown in Tables D.1-D.6; 127 terms corresponds to $N = M = 5$, 247 terms to $N = M = 7$ and 407 terms to $N = M = 9$. The chosen basic value of N_x is 150 N/mm for layups A1 and B1, and 250 N/mm for layups A2 and B2. For layups A3 and B3, N_x is set to 500 N/mm. For layups A4 and B4, N_x is set to 1000 N/mm. The remaining layups are implemented with $N_x = 2000$ N/mm.

Table D.1
Ply region degradation model (PRDM-DF1) for Case A (triaxial layup).

Imp. % of b	t (mm)	No. of plies (no. of ply regions)	No. of terms	$\Delta\eta$	σ_{FPF} (MPa)	σ_{max} (MPa)	σ_{max_ref} (MPa)	$\frac{\sigma_{max}}{\sigma_{max\_ref}}$
0.1	10.02	34 (306)	407	0.05	39.86	110.02	130	0.85
0.1	16.70	34 (306)	407	0.10	84.79	140.26	180	0.78
0.1	24.94	34 (306)	127	0.10	172.00	182.54	240	0.76
0.1	33.40	34 (306)	127	0.10	271.31	308.72	320	0.96
0.1	49.98	34 (306)	127	0.10	382.13	570.09	570	1.00
1.0	10.02	34 (306)	407	0.05	31.64	109.77	130	0.84
1.0	16.70	34 (306)	407	0.10	45.91	139.42	180	0.77
1.0	24.94	34 (306)	247	0.10	71.39	193.35	235	0.82
1.0	33.40	34 (306)	247	0.10	97.29	267.01	300	0.89
1.0	49.98	34 (306)	127	0.10	149.55	399.82	435	0.92
2.0	10.02	34 (306)	407	0.05	25.90	108.17	130	0.83
2.0	16.70	34 (306)	407	0.10	35.79	134.12	178	0.75
2.0	24.94	34 (306)	247	0.10	46.69	184.08	225	0.82
2.0	33.40	34 (306)	247	0.10	60.04	244.69	280	0.87
2.0	49.98	34 (306)	127	0.10	87.52	368.29	395	0.93
3.0	10.02	34 (306)	407	0.05	22.96	108.52	130	0.83
3.0	16.70	34 (306)	407	0.10	30.37	129.36	174	0.74
3.0	24.94	34 (306)	247	0.10	38.92	179.61	218	0.82
3.0	33.40	34 (306)	247	0.10	46.19	230.80	260	0.89
3.0	49.98	34 (306)	127	0.10	64.26	341.32	360	0.95

Table D.2
Ply region degradation model (PRDM-DF1) for Case B (quadriaxial layup).

Imp. % of b	t (mm)	No. of plies (no. of ply regions)	No. of terms	$\Delta\eta$	σ_{FPF} (MPa)	σ_{max} (MPa)	σ_{max_ref} (MPa)	$\frac{\sigma_{max}}{\sigma_{max\_ref}}$
0.1	8.00	8 (72)	407	0.05	29.08	108.12	105	1.03
0.1	16.00	16 (144)	407	0.10	83.19	162.06	180	0.90
0.1	24.00	24 (216)	247	0.10	170.92	206.88	215	0.96
0.1	32.00	32 (288)	247	0.10	198.40	259.99	270	0.96
0.1	48.00	48 (432)	247	0.10	204.13	307.42	340	0.90
1.0	8.00	8 (72)	407	0.05	27.38	108.03	107	1.01
1.0	16.00	16 (144)	407	0.10	43.80	160.11	181	0.88
1.0	24.00	24 (216)	247	0.10	69.49	195.89	210	0.93
1.0	32.00	32 (288)	247	0.10	94.30	232.98	240	0.97
1.0	48.00	48 (432)	247	0.10	144.77	271.95	302	0.90
2.0	8.00	8 (72)	407	0.05	26.68	108.55	108	1.01
2.0	16.00	16 (144)	407	0.10	33.03	158.14	181	0.87
2.0	24.00	24 (216)	247	0.10	44.22	191.18	205	0.93
2.0	32.00	32 (288)	247	0.10	57.58	219.57	230	0.95
2.0	48.00	48 (432)	247	0.10	84.87	243.79	270	0.90
3.0	8.00	8 (72)	407	0.05	26.08	109.67	115	0.95
3.0	16.00	16 (144)	407	0.10	29.90	156.77	185	0.85
3.0	24.00	24 (216)	247	0.10	35.62	187.14	205	0.91
3.0	32.00	32 (288)	247	0.10	43.32	211.14	222	0.95
3.0	48.00	48 (432)	247	0.10	61.70	248.63	260	0.96

Table D.3
Ply region degradation model (PRDM-DF2) for Case A (triaxial layup).

Imp. % of b	t (mm)	No. of plies (no. of ply regions)	No. of terms	$\Delta\eta$	σ_{FPF} (MPa)	σ_{max} (MPa)	σ_{max_ref} (MPa)	$\frac{\sigma_{max}}{\sigma_{max\_ref}}$
0.1	10.02	34 (306)	407	0.05	42.50	117.75	130	0.91
0.1	16.70	34 (306)	407	0.10	86.95	189.87	180	1.05
0.1	24.94	34 (306)	127	0.10	173.39	241.86	240	1.01
0.1	33.40	34 (306)	127	0.10	272.81	314.71	320	0.98
0.1	49.98	34 (306)	127	0.10	382.14	577.57	570	1.01
1.0	10.02	34 (306)	407	0.05	40.37	117.02	130	0.90
1.0	16.70	34 (306)	407	0.10	53.03	187.09	180	1.04
1.0	24.94	34 (306)	247	0.10	77.65	236.25	235	1.01
1.0	33.40	34 (306)	247	0.10	103.27	290.35	300	0.97
1.0	49.98	34 (306)	127	0.10	155.05	401.84	435	0.92
2.0	10.02	34 (306)	407	0.05	39.37	116.31	130	0.89
2.0	16.70	34 (306)	407	0.10	46.29	184.00	178	1.03
2.0	24.94	34 (306)	247	0.10	55.59	232.92	225	1.04
2.0	33.40	34 (306)	247	0.10	68.46	279.28	280	1.00
2.0	49.98	34 (306)	127	0.10	95.03	364.81	395	0.92
3.0	10.02	34 (306)	407	0.05	38.08	115.95	130	0.89
3.0	16.70	34 (306)	407	0.10	43.87	181.49	174	1.04
3.0	24.94	34 (306)	247	0.10	49.57	224.60	218	1.03
3.0	33.40	34 (306)	247	0.10	56.11	268.87	260	1.03
3.0	49.98	34 (306)	127	0.10	73.02	342.20	360	0.95

Table D.4
Ply region degradation model (PRDM-DF2) for Case B (quadriaxial layup).

Imp. % of b	t (mm)	No. of plies (no. of ply regions)	No. of terms	$\Delta\eta$	σ_{FPF} (MPa)	σ_{max} (MPa)	σ_{max_ref} (MPa)	$\frac{\sigma_{max}}{\sigma_{max\_ref}}$
0.1	8.00	8 (72)	407	0.05	32.47	110.09	105	1.05
0.1	16.00	16 (144)	407	0.10	84.56	159.97	180	0.89
0.1	24.00	24 (216)	247	0.10	171.83	205.08	215	0.95
0.1	32.00	32 (288)	247	0.10	198.40	261.02	270	0.97
0.1	48.00	48 (432)	247	0.10	204.13	307.42	340	0.90
1.0	8.00	8 (72)	407	0.05	32.15	111.36	107	1.04
1.0	16.00	16 (144)	407	0.10	48.38	157.87	181	0.87
1.0	24.00	24 (216)	247	0.10	74.17	190.01	210	0.90
1.0	32.00	32 (288)	247	0.10	98.79	228.49	240	0.95
1.0	48.00	48 (432)	247	0.10	148.93	265.21	302	0.88
2.0	8.00	8 (72)	407	0.05	34.04	113.33	108	1.05
2.0	16.00	16 (144)	407	0.10	38.71	155.31	181	0.86
2.0	24.00	24 (216)	247	0.10	50.21	181.87	205	0.89
2.0	32.00	32 (288)	247	0.10	63.63	211.57	230	0.92
2.0	48.00	48 (432)	247	0.10	90.86	257.64	270	0.95
3.0	8.00	8 (72)	407	0.05	36.24	118.09	115	1.03
3.0	16.00	16 (144)	407	0.10	35.69	152.86	185	0.83
3.0	24.00	24 (216)	247	0.10	42.13	174.92	205	0.85
3.0	32.00	32 (288)	247	0.10	49.95	200.47	222	0.90
3.0	48.00	48 (432)	247	0.10	68.47	245.32	260	0.94

Table D.5
Strength predictions for layup cases C and D using PRDM-DF1.

Layup case	Imp. % of b	t (mm)	No. of plies (no. of ply regions)	No. of terms	N_x (N/mm)	$\Delta\eta$	σ_{max} (MPa)	σ_{max_ref2} (MPa)	$\frac{\sigma_{max}}{\sigma_{max\_ref2}}$
C1	0.1	10.00	24 (216)	407	150	0.05	119.08	129	0.92
C2	0.1	16.70	24 (216)	407	200	0.10	156.05	162	0.96
C3	0.1	25.00	24 (216)	247	500	0.10	223.30	220	1.02
C4	0.1	33.30	24 (216)	247	1000	0.10	283.46	298	0.95
C5	0.1	50.00	24 (216)	127	2000	0.10	321.03	343	0.94
D1	0.1	10.00	24 (216)	407	150	0.05	143.72	137	1.05
D2	0.1	16.70	24 (216)	407	200	0.10	203.01	215	0.94
D3	0.1	25.00	24 (216)	247	500	0.10	179.12	259	0.69
D4	0.1	33.30	24 (216)	247	1000	0.10	301.11	306	0.98
D5	0.1	50.00	24 (216)	247	2000	0.10	552.57	543	1.02

Table D.6
Strength predictions for layup cases C and D using PRDM-DF2.

Layup case	Imp. % of b	t (mm)	No. of plies (no. of ply regions)	No. of terms	N_x (N/mm)	$\Delta\eta$	σ_{max} (MPa)	σ_{max_ref2} (MPa)	$\frac{\sigma_{max}}{\sigma_{max\_ref2}}$
C1	0.1	10.00	24 (216)	407	150	0.05	103.55	129	0.80
C2	0.1	16.70	24 (216)	407	200	0.10	142.14	162	0.88
C3	0.1	25.00	24 (216)	247	500	0.10	219.19	220	1.00
C4	0.1	33.30	24 (216)	247	1000	0.10	282.26	298	0.95
C5	0.1	50.00	24 (216)	127	2000	0.10	316.05	343	0.92
D1	0.1	10.00	24 (216)	407	150	0.05	170.53	137	1.24
D2	0.1	16.70	24 (216)	407	200	0.10	209.73	215	0.98
D3	0.1	25.00	24 (216)	247	500	0.10	244.78	259	0.95
D4	0.1	33.30	24 (216)	247	1000	0.10	313.92	306	1.03
D5	0.1	50.00	24 (216)	247	2000	0.10	554.39	543	1.02